RelA-SpoT Homologue toxins pyrophosphorylate the CCA end of tRNA to inhibit protein synthesis

Tatsuaki Kurata[1*], Tetiana Brodiazhenko[2], Sofia Raquel Alves Oliveira[2], Mohammad Roghanian[1,3,4], Kathryn Jane Turnbull[3,4], Ondřej Bulvas[5], Hiraku Takada[6], Hedvig Taman[7], Andres Ainelo[7], Radek Pohl[5], Dominik Rejman[5], Tanel Tenson[2], Abel Garcia-Pino[7,8], Gemma C. Atkinson[1*], Vasili Hauryliuk[1,2,3,9*]

[1]Department of Experimental Medical Science, Lund University, 221 00 Lund, Sweden
[2]University of Tartu, Institute of Technology, 50411 Tartu, Estonia
[3]Laboratory for Molecular Infection Medicine Sweden (MIMS), Umeå University, SE-901 87 Umeå, Sweden
[4]Department of Clinical Microbiology, Rigshospitalet, 2200 Copenhagen, Denmark
[5]Institute of Organic Chemistry and Biochemistry, Academy of Sciences of the Czech Republic, v.v.i., Flemingovonam. 2, CZ-166 10 Prague 6, Czech Republic
[6]Faculty of Life Sciences, Kyoto Sangyo University, Kamigamo, Motoyama, Kita-ku, Kyoto 603-8555, Japan
[7]Cellular and Molecular Microbiology (CM2), Faculté des Sciences, Université Libre de Bruxelles (ULB), Campus La Plaine, Building BC, Room 1C4203, Boulevard du Triomphe, 1050, Brussels, Belgium
[8]WELBIO, Avenue Hippocrate 75, 1200 Brussels, Belgium
[9]Lead Contact

[*]Correspondence to: tatsuaki.kurata@med.lu.se, gemma.atkinson@med.lu.se, vasili.hauryliuk@med.lu.se

Summary: RelA-SpoT Homolog (RSH) enzymes control bacterial physiology through synthesis and degradation of the nucleotide alarmone (p)ppGpp. We recently discovered multiple families of Small Alarmone Synthetase (SAS) RSH acting as toxins of toxin-antitoxin (TA) modules, with the FaRel subfamily of toxSAS abrogating bacterial growth by producing an analogue of (p)ppGpp, (pp)pApp. Here we probe the mechanism of growth arrest employed by four experimentally unexplored subfamilies of toxSAS: FaRel2, PhRel, PhRel2 and CapRel. Surprisingly, all these toxins specifically inhibit protein synthesis. To do so, they transfer a pyrophosphate moiety from ATP to the tRNA 3′ CCA. The modification inhibits both tRNA aminoacylation and the sensing of cellular amino acid starvation by the ribosome-associated RSH RelA. Conversely, we show that some Small Alarmone Hydrolase (SAH) RSH enzymes can reverse the pyrophosphorylation of tRNA to counter the growth inhibition by toxSAS. Collectively, we establish RSHs as a novel class of RNA-modifying enzymes.

Keywords: RelA-SpoT Homolog, toxin antitoxin, tRNA modification, translation, (p)ppGpp

Introduction

Toxin–antitoxin (TA) systems are a class of highly diverse and widespread small operons found in bacterial, archaeal and bacteriophage genomes (Fraikin et al., 2020; Harms et al., 2018). TAs have a broad range of functions, including bacterial defence against bacteriophages, phage competition for infection of bacteria, stabilization of transposons, plasmids and bacterial genomes – all of which rely on the highly potent toxicity of the protein toxin controlled by the protein- or RNA-based antitoxin (Blower et al., 2009; Fiedoruk et al., 2015; Jaffe et al., 1985; Lima-Mendez et al., 2020; Song and Wood, 2020). Many TA toxins are closely evolutionary related to housekeeping enzymes, suggesting a 'breakaway' evolutionary path on which a generally harmless enzyme evolves a toxic function that requires tight control by the antitoxin (Burckhardt and Escalante-Semerena, 2020; Garcia-Pino et al., 2014; Jimmy et al., 2020; Koonin and Makarova, 2019; Senissar et al., 2017).

The RelA-SpoT Homolog (RSH) protein family of housekeeping stress-response enzymes was only recently recognised to also contain TA toxins (Jimmy et al., 2020). The function of housekeeping RSHs is to control the cellular levels of alarmone nucleotides ppGpp (guanosine-3′,5′-bisdiphosphate) and pppGpp (guanosine-5′-triposphate-3′-diphosphate) – collectively referred to as (p)ppGpp – with the alarmones, in turn, regulating metabolism, virulence and growth rate, as well as playing an important role in antibiotic and stress tolerance (Gaca et al., 2015; Hauryliuk et al., 2015; Irving et al., 2020; Liu et al., 2015; Zhu et al., 2019). RSH family members can both synthesise (p)ppGpp by transferring the pyrophosphate group of ATP to the 3′ position of either GDP or GTP, and convert it back to GDP/GTP through removal of the 3′ pyrophosphate (Atkinson et al., 2011; Cashel and Gallant, 1969). RSHs can be classified into long multi-domain RSHs – with the archetypical representatives being *Escherichia coli* enzymes RelA (Haseltine and Block, 1973) and SpoT (Xiao et al., 1991) – and short single-domain RSHs (Atkinson et al., 2011). The latter are highly diverse, and can be subdivided into Small Alarmone Synthetases (SAS; 30 distinct subfamilies, with numerous experimentally representatives extensively characterised, including *Staphylococcus aureus* RelP (Geiger et al., 2014; Manav et al., 2018) and *Bacillus subtilis* RelQ (Nanamiya et al., 2008; Steinchen et al., 2015)) and Small Alarmone Hydrolases (SAH; 11 subfamilies) (Jimmy et al., 2020).

Several recent discoveries have sparked interest in how non-(p)ppGpp RSH-mediated chemical catalysis can be weaponised by bacteria for potent growth inhibition. Highly toxic SAS RSH enzymes that are injected by secretion systems (Ahmad et al., 2019) or constitute the

toxic components (toxSAS), of toxin-antitoxin (TA) modules (Jimmy et al., 2020) were found to produce a structural analogue of (p)ppGpp – pApp, ppApp and pppApp – collectively constituting (pp)pApp (**Figure S1**). By abrogating *de novo* purine synthesis through orthosteric inhibition of PurF (Ahmad et al., 2019), (pp)pApp inhibits translation, transcription and replication (Jimmy et al., 2020). SAHs have also been shown to catalyse unexpected new reactions. While no (p)ppGpp synthetases are encoded in mammalian genomes, human MESH1 was identified in 2010 as an efficient (p)ppGpp hydrolase (Sun et al., 2010). A decade later, compelling evidence was presented that human MESH1 is a NADPH phosphatase (Ding et al., 2020). Combined with the dramatic evolutionary diversity of this largely experimentally unexplored protein family (Atkinson et al., 2011; Jimmy et al., 2020), these discoveries demonstrate that RSH-mediated catalysis is versatile and that the biological functions of RSH enzymes are clearly not limited to (p)ppGpp metabolism.

We have recently experimentally validated representatives of five toxSAS subfamilies as *bona fide* TA effectors: *Cellulomonas marina* FaRel, *Bacillus subtilis* la1a PhRel2, *Coprobacillus* sp. D7 FaRel2, *Mycobacterium* phage Phrann PhRel (Gp29) and *Mycobacterium tuberculosis* AB308 CapRel (Jimmy et al., 2020). Out of these, only the (pp)pApp-producing *C. marina* FaRel was previously functionally characterised. In this study we uncover surprising non-alarmone chemistry catalysed by previously unexplored FaRel2, PhRel2, PhRel and CapRel enzymes as well as shed light on how the toxicity of non-alarmone toxSASs can be counteracted through the hydrolytic activity of SAHs.

Results

Representatives of FaRel2, PhRel, PhRel2 and CapRel toxSAS subfamilies specifically inhibit protein synthesis

While the mechanism of toxicity employed by PhRel, PhRel2, FaRel2 and CapRel toxSAS subfamilies is as yet uncharacterised, we initially assumed that these toxSASs – just as *C. marina* FaRel TA toxin (Jimmy et al., 2020) and the Tas1 toxic RSH effector of *Pseudomonas aeruginosa* Type VI secretion system (Ahmad et al., 2019) – inhibit bacterial growth by producing (pp)pApp. Surprisingly, when we analysed the nucleotide pools of growth-arrested *E. coli* expressing *B. subtilis* la1a PhRel2, we detected no accumulation of (pp)pApp (**Figure 1A** and **Figure S1D**). At the same time, we robustly detected (pp)pApp upon expression of FaRel (**Figure S1E**; the synthesis of (pp)pApp standards is described on **Figure S2**). Similarly, we did not detect (pp)pApp upon expression of *Coprobacillus* sp. D7 FaRel2 either (**Figure S1H**). These results suggested that toxSASs might not universally act via production of (pp)pApp, and therefore, multiple toxSAS subfamilies could have a mechanism of toxicity distinct from that of FaRel and Tas1.

We used metabolic labelling to uncover the effects of as yet uncharacterised toxSASs on translation (by following incorporation of ^{35}S-methionine in proteins), transcription (incorporation of ^{3}H-uridine in RNA) and replication (incorporation of ^{3}H-thymidine in DNA). In stark contrast to FaRel (Jimmy et al., 2020) and Tas1 (Ahmad et al., 2019) which both inhibit all the three processes (**Figure S3A**), representatives of all four unexplored toxSAS subfamilies specifically inhibited translation. The strongest inhibition was observed for *B. subtilis* la1a PhRel2 and *Coprobacillus* sp. D7 FaRel2 (**Figure 1C,B**), while *M. tuberculosis* AB308 CapRel and *Mycobacterium* phage Phrann superinfection immunity protein PhRel (Gp29) (Dedrick et al., 2017) had a weaker, but still specific effect on protein synthesis (**Figure S3B,C**). Interestingly, upon induction of FaRel2, ^{3}H-uridine incorporation increased. This is likely due to abrogation of ATP consumption upon cessation of translation, resulting in increased transcription; we earlier observed a similar effect upon specific inhibition of translation by the antibiotic kanamycin (Jimmy et al., 2020). Collectively, our results suggested that specific inhibition of translation is a common mode of toxSAS toxicity, with the FaRel toxSAS subfamily deviating from this common *modus operandi*.

We next tested whether inhibition of translation by toxSASs is mediated by a direct mechanism using production of dihydrofolate reductase, DHFR, in a reconstituted cell-free protein synthesis system from *E. coli* components (PURE) (Shimizu et al., 2001) as a readout

of toxSAS activity. Although purification of toxSAS enzymes is exceedingly challenging (Jimmy et al., 2020), we succeeded in purifying enzymatically-competent C-terminally $FLAG_3$-tagged *Coprobacillus* sp. D7 FaRel2 toxin through α-$FLAG_3$-immunoprecipitation (**Figure S4**). As we have shown earlier, the $FLAG_3$-tag does not interfere with toxicity of FaRel2 or the ability of the antitoxin to counteract the protein (Jimmy et al., 2020). As a specificity control, we used catalytically compromised FaRel2 variants Y128A (predicted to disrupt the stacking interaction with the pyrophosphate acceptor substrate (Steinchen et al., 2018)) and D90G (predicted to compromise the coordination of the Mg^{2+} ion (Steinchen et al., 2015)). Both of the substituted residues are highly conserved amongst SAS RSH enzymes (**Figure S5A**) and mutant variants are non-toxic when expressed in *E. coli* (**Figure 1D**). The addition of wild-type – but not D90G or Y128A – FaRel2 to the PURE system abrogated DHFR production (**Figure 1E**, **Figure S6A**). The addition of the ATfaRel2 antitoxin which acts though sequestering FaRel2 into inactive complex (Jimmy et al., 2020) counteracted the inhibitory effect of FaRel2 (**Figure 1F**). We concluded that this toxSAS, indeed, directly targets the protein synthesis machinery.

Coprobacillus sp. D7 FaRel2 specifically modifies the tRNA 3′ CCA end to abrogate aminoacylation

Inhibition of protein production is a common means of toxicity in TA systems, with the toxic components often acting via modification of tRNA, such as cleavage (employed by VapC toxins (Cruz et al., 2015; Winther and Gerdes, 2011)), acetylation of the attached amino acid (as seen with GNAT toxins (Cheverton et al., 2016; Jurenas et al., 2017)) or inactivation of the 3′ CCA end through the addition of pyrimidines (employed by $MenT_3$ (Cai et al., 2020)). RSH enzymes have never previously been shown to catalyse synthesis of any other products than hyperphosphorylated nucleotides (pp)pGpp and (pp)pApp. However, one could imagine that the pyrophosphate group of the ATP donor could be transferred onto the ribose position of the 3′ terminal adenosine of tRNA instead of the corresponding 3′ ribose position of the ATP/ADP substrate used by Tas1/FaRel to produce (pp)pApp. Since the availability of this 3′ hydroxyl group is essential for tRNA aminoacylation, the modification would efficiently inhibit protein synthesis.

We tested this hypothesis using deacylated *E. coli* tRNA as a substrate and γ-^{32}P ATP as a donor of radioactively labelled pyrophosphate moiety. In the presence of γ-^{32}P ATP FaRel2

efficiently radiolabels both initiator $tRNA_i^{fMet}$ (**Figure 2A,B**) and elongator $tRNA^{Phe}$ (**Figure 2B**). The tRNA-labelling activity is lost in D90G and Y128A FaRel variants (**Figure 2C**), and is specifically counteracted by both the AtFaRel2 Type II antitoxin and tRNA aminoacylation (**Figure 2D,E**). The latter result strongly suggests that the ^{32}P label is transferred by FaRel2 onto the 3′ hydroxyl group of the tRNA terminal adenine residue that acts as an amino acid acceptor. To probe this experimentally, we tested the effect of tRNA modification by FaRel2 on aminoacylation of $tRNA^{Phe}$. The aminoacylation reaction was readily abrogated by FaRel2 (**Figure 2F**) in a strictly ATP-dependent manner (**Figure 2G**), thus explaining the molecular mechanism of translational arrest by this toxSAS. In principle, the FaRel2-modified phospho-tRNA might not just be incompetent in aminoacylation, but also actively toxic to translation due to, for instance, stable binding to the ribosomal A-site or elongation factor EF-Tu. To test this hypothesis, we first titrated total tRNA in the PURE system and identified the near-saturating tRNA concentration (50 μM) at which, we reasoned, the system would be most sensitive to inhibition (**Figure S6B**). However, added in concentrations up to 14 μM, phospho-$tRNA^{Phe}$ had no effect on DHFR synthesis (**Figure S6C**), suggesting that while phospho-tRNA is translation-incompetent, it is not inhibitory to the protein synthesis machinery. Rather, the toxicity likely results from a depletion of chargeable tRNA in the cell.

To test the generality of toxSAS-mediated translation inhibition via tRNA CCA pyrophosphorylation, we purified and tested *B. subtilis* la1a PhRel2. Similarly to *Coprobacillus* FaRel2, PhRel2 efficiently abrogates protein synthesis in the PURE system (**Figure S6D**) and γ-^{32}P-labels both $tRNA_i^{fMet}$ and $tRNA^{Phe}$ (**Figure S6E**).

Finally, we assessed the specificity of tRNA modification by FaRel2. Both deacylated initiator $tRNA_i^{fMet}$ and elongator $tRNA^{Phe}$ were labelled with ^{32}P by FaRel2 (**Figure 2B**), which suggests that the 3′ CCA could be sufficient for recognition of deacylated tRNA. To test this hypothesis and probe the specificity of the toxSAS for tRNA's 3′ adenine residue we performed radiolabelling experiments with a set of synthetic 5′-CACCN-3′ RNA pentanucleotides containing both the 3′ A as well as 3′ C, G and U (**Figure 2H**). Only one of the four RNA substrates, CACCA, was labelled with ^{32}P, suggesting specificity for 3′ adenine. At the same time, the CACCA DNA oligonucleotide did not serve as a FaRel2 substrate, suggesting a functional importance of the 2′ hydroxyl group of the 3′ adenine (**Figure 2H**). This result is in good agreement with a recent report demonstrating that (p)ppGpp-synthesising RSH enzymes cannot catalyse the transfer of the pyrophosphate group of the ATP donor to dGTP instead of the GTP substrate (Patil et al., 2020).

tRNA 3′ CCA end modification by FaRel2 abrogates ribosome-dependent activation of (p)ppGpp synthesis by amino acid starvation sensor RelA

In Gammaproteobacteria such as *E. coli,* amino acid limitation is sensed by a housekeeping multidomain RSH enzyme RelA (Atkinson et al., 2011). This ribosome-associated factor inspects the aminoacylation status of the 3′ CCA of the A-site tRNA (Arenz et al., 2016; Brown et al., 2016; Loveland et al., 2016), and, upon detecting deacylated tRNA, synthesises the (p)ppGpp alarmone (Haseltine and Block, 1973). While the free 3′ OH moiety of the terminal adenosine residue is essential for full activation of RelA's synthesis activity by tRNA on the ribosome (Sprinzl and Richter, 1976), RelA is still activated by the 70S ribosome, although to a lesser extent if activation by tRNA is compromised by the antibiotics thiostrepton (Kudrin et al., 2017) and tetracycline (Kudrin et al., 2018).

Using a reconstituted *E. coli* biochemical system (Kudrin et al., 2018) we tested the effect of FaRel2 on RelA activation by deacylated tRNA of starved ribosomal complexes (**Figure 2J**). FaRel2 efficiently abrogated activation of RelA by tRNA, reducing RelA activity to the levels observed in the presence of 70S initiation complexes lacking the A-site deacylated tRNA. Thus, not only does FaRel2 *not* produce an alarmone, it also could prevent the housekeeping RSH cellular machinery from being activated by starved ribosomes to produce the (p)ppGpp alarmone.

Small Alarmone Synthetase (SAH) RSH enzymes can restore tRNA aminoacylation competence of FaRel2-modified tRNA

When co-expressed with *Coprobacillus* FaRel2, human MESH1 and *C. marina* ATfaRel hydrolysis-only Small Alarmone Synthetase (SAH) enzymes can efficiently counteract the growth inhibition by the toxSAS (**Figure 3A**) (Jimmy et al., 2020). This detoxification activity suggests that MESH1 and ATfaRel can recycle pyrophosphorylated tRNA back to translation-competent deacylated tRNA.

To probe this conjecture experimentally, we pyrophosphorylated $tRNA^{Phe}$ *Coprobacillus* FaRel2, isolated the modified tRNA, and tested whether the human MESH1, *C. marina* ATfaRel or cognate Type II *Coprobacillus* AtFaRel2 Type II antitoxin (not an SAH) could restore the aminoacylation activity of pyrophosphorylated $tRNA^{Phe}$ (**Figure 3B**). In excellent agreement with our microbiological results (Jimmy et al., 2020) and consistent with

CCA pyrophosphorylation being the cause of growth arrest by FaRel2, both tested SAH enzymes restore the $tRNA^{Phe}$ aminoacylation. At the same time, we detected no effect upon the addition of the ATfaRel2 antitoxin which neutralises FaRel2 by sequestering the toxSAS into an inactive complex (Jimmy et al., 2020), and, therefore, is not expected to restore the aminoacylation competence of FaRel2-modified tRNA.

Mapping the tRNA 3′ CCA interaction by FaRel2 through molecular docking and mutagenesis

To gain structural insight into the mechanism of tRNA substrate recognition by FaRel2, we used the Rosetta suite (Song et al., 2013) to model the structure of *Coprobacillus* FaRel2 based on the structures of *S. aureus* housekeeping SAS RelP (Manav et al., 2018) and *B. subtilis* SAS RelQ (Steinchen et al., 2015), PDBIDs 6FGK and 6EWZ, respectively. The model predicted by Rosetta was then used to dock deacylated $tRNA^{Phe}$ into the active site as implemented in the HADDOCK suite (van Zundert et al., 2016). As the only distance restraint in the docking experiment we used the necessary proximity of FaRel2 Y128 to the CCA-adenine.

The resulting model of the FaRel2-tRNA complex reveals that a cluster of basic residues accommodate the acceptor stem guiding the CCA end into the active site of the enzyme (**Figure 4A**). In such arrangement, the orientation of the 3′-adenosine is reminiscent of the way GDP is coordinated in the active site of housekeeping SAS *S. aureus* RelP (Manav et al., 2018), next to the binding site of ATP, the pyrophosphate donor. Conversely, the analysis of the electrostatic surface profile of RelP and RelQ shows a charge reversal in the same region (**Figure S5BC**). The presence of a more acidic region in these SASs correlates with a lack of tRNA-pyrophosphorylation activity of these enzymes which would likely be incompatible with tRNA binding.

We probed our molecular model through point mutations in this recognizable basic patch, using FaRel2 toxicity as a readout of intact efficient tRNA recognition (**Figure 4B**). As predicted from our model, Ala-substitutions in the basic cluster located towards the N-terminus of the toxin that includes K28 and K29 abolished the toxicity of FaRel2. Ala-substitutions in the outside rim of the active site (including R114 and Y134) which were predicted to contact the tRNA in our interaction model also compromise the toxicity of FaRel2. These residues are all outside the active site and would not be involved directly in catalysis, thus their effect on toxicity is likely related with tRNA binding. Finally, as a control we confirmed that Ala-

substitution of basic residues throughout the surface of FaRel2 had no effect on toxicity (**Figure 4B**).

Discussion

TA toxins belonging to the same protein family can display relaxed specificity towards their targets (Goeders et al., 2013; Harms et al., 2018; Page and Peti, 2016; Schureck et al., 2015; Yamaguchi and Inouye, 2009) or even enzymatically modify clearly distinct classes of substrates (Burckhardt and Escalante-Semerena, 2020; Castro-Roa et al., 2013; Harms et al., 2015; Jurenaite et al., 2013; Jurenas et al., 2017). A classic example is the GCN5-related N-acetyltransferase (GNAT) TA toxins – a versatile family of enzymes unrelated to RSHs. While GNAT TA toxins inhibit protein synthesis by acetylating aminoacyl-tRNAs (Cheverton et al., 2016; Jurenas et al., 2017), the majority of non-toxic GNATs modify small molecules such as polyamines, antibiotics, phospholipids and amino acids (Burckhardt and Escalante-Semerena, 2020). This substrate specificity spectrum – toxicity mediated via tRNA modification combined with non-toxic modification of small molecule substrates – is strikingly similar to what we present here for RSH enzymes.

Our results uncover a novel enzymatic activity of some toxSAS RSHs to efficiently abrogate translation. We propose the following model of substrate specificity change within the diversity synthetase-competent RSH enzymes (**Figure 5**). The vast majority of RSH synthetases specifically recognise the guanosine residue of the nucleotide (GTP or GDP) substrate to catalyse the synthesis of the housekeeping alarmone (p)ppGpp (**Figure 5A**). In toxic SAS enzymes such *C. marina* FaRel and *P. aeruginosa* Tas1, the substrate specificity is either relaxed, allowing synthesis of both (p)ppGpp and (pp)pApp (toxSAS FaRel (Jimmy et al., 2020)) or switched to specific synthesis of (pp)pApp (Tas1 (Ahmad et al., 2019)) (**Figure 5A**).

Translation-inhibiting toxSASs belong to SAS subfamilies that are found in various major phyla of Gram-positive and -negative bacteria, including Firmicutes, Actinobacteria, Proteobacteria, Bacteroidetes, Acidobacteria, Planctomycetes and Cyanobacteria, as well as multiple bacteriophages and even some archaea (Jimmy et al., 2020). Sequence alignment of the SYNTH domain of toxSASs and other SASs shows that while there are strongly differentially conserved motifs in (pp)pApp-synthesising toxSASs relative to other RSHs, there is – surprisingly – not a clear sequence signature of toxSASs that use tRNA as a substrate (**Figure S5**). Indeed, there is no particular support for monophyly of all toxSASs targeting

translation in phylogenetic analysis of RSHs (although there is support for two monophyletic clades comprising FpRel2+PhRel2+FaRel2 and CapRel+PhRel) (Jimmy et al., 2020). The position of the tRNA accepting toxSAS clades at roughly the midpoint of the RSH tree tempts us to speculate that the ancestral function of the SYNTH domain at a time predating the last universal common ancestor (LUCA) could have been pyrophosphorylation of RNA, rather than (pp)pNpp synthesis.

Perspective and limitations

With 30 distinct SAS subfamilies identified to date (Jimmy et al., 2020), it is likely we are yet to discover the full spectrum of chemical reactions catalysed by the evolutionary versatile RSH synthetase domain. As we show here, pyrophosphorylated tRNA 3′ CCA end can serve as a substrate for SAH enzymes human MESH1 and *C. marina* ATfaRel (**Figure 3B**). This expands the spectrum of known hydrolysis reactions catalysed by RSH beyond hydrolysis of (pyro)phosphorylated nucleotides, indicating a possible new role of RSH hydrolases as RNA-modifying enzymes with a 3′-phosphatase activity similar to that of T4 polynucleotide kinase, Pnk.

This study lays the foundations for the future studies of the non-alarmone chemistry catalysed by bacterial and viral RSH enzymes. Dedicated structural studies are essential for further rationalising our results on the molecular level. All of the experiments presented in the current study are rely on heterologous expression in *E. coli* or utilise reconstituted biochemical system from *E. coli* components. In order to understand the biological roles of toxSAS TAs it will be essential to study these effectors and the antitoxins neutralising them in native bacterial and viral hosts.

ACKNOWLEDGMENTS

We are grateful to Protein Expertise Platform (PEP) at Umeå University and Mikael Lindberg for constructing plasmids, Andrey Chabes, Nasim Sabouri and Ikenna Obi for providing γ-^{32}P ATP, to Steffi Jimmy and Constantine Stavropoulos their contributions at the initial stages of this project. This work was supported by the funds from European Regional Development Fund through the Centre of Excellence for Molecular Cell Technology (VH and TT, 2014-2020.4.01.15-0013); the Molecular Infection Medicine Sweden (MIMS) (VH); The Estonian Research Council (PRG335 to TT and VH); The Swedish Research Council (Vetenskapsrådet; 2017-03783 to VH and 2019-01085 to GCA); The Ragnar Söderberg foundation (VH); MIMS

322 Excellence by Choice Postdoctoral Fellowship Programme (postdoctoral grant 2018 to MR);
323 The Kempe Foundation (SMK-1858.3 to GCA); Carl Tryggers Stiftelse för Vetenskaplig
324 Forskning (19-24 to GCA). The Czech ministry of Education and Sport (grant number 8F19006
325 to DR) and the Swedish Research Council (2018-00956 to VH) within the RIBOTARGET
326 consortium under the framework of JPIAMR; Umeå Centre for Microbial Research (UCMR)
327 (postdoctoral grant 2017 to HT); the Fonds National de Recherche Scientifique [FRFS-
328 WELBIO CR-2017S-03, FNRS CDR J.0068.19, FNRS-PDR T.0066.18]; Joint Programming
329 Initiative on Antimicrobial Resistance [JPI-EC-AMR -R.8004.18]; Program 'Actions de
330 Recherche Concerté 2016–2021 and Fonds d'Encouragement à la Recherche (FER) of ULB;
331 Fonds Jean Brachet, the Fondation Van Buuren and the ERC CoG DiStRes (Grant Agreement
332 n° 864311) to A.G.P.; the European postdoctoral programme (Marie Skłodowska Curie
333 COFUND action) to A.A..
334

335 **AUTHOR CONTRIBUTIONS**

336 VH coordinated the study and drafted the manuscript with contributions from all authors. TK,
337 AGP and VH designed experiments and analysed the data.TK, TB, SRAO, MR, KJT, OB, HT,
338 AA, HTaman performed experiments. DR, RP, TT and AGP provided reagents. GCA
339 performed bioinformatic analyses.
340

341 **DECLARATION OF INTERESTS**

342 The authors declare no competing interests.
343

FIGURES

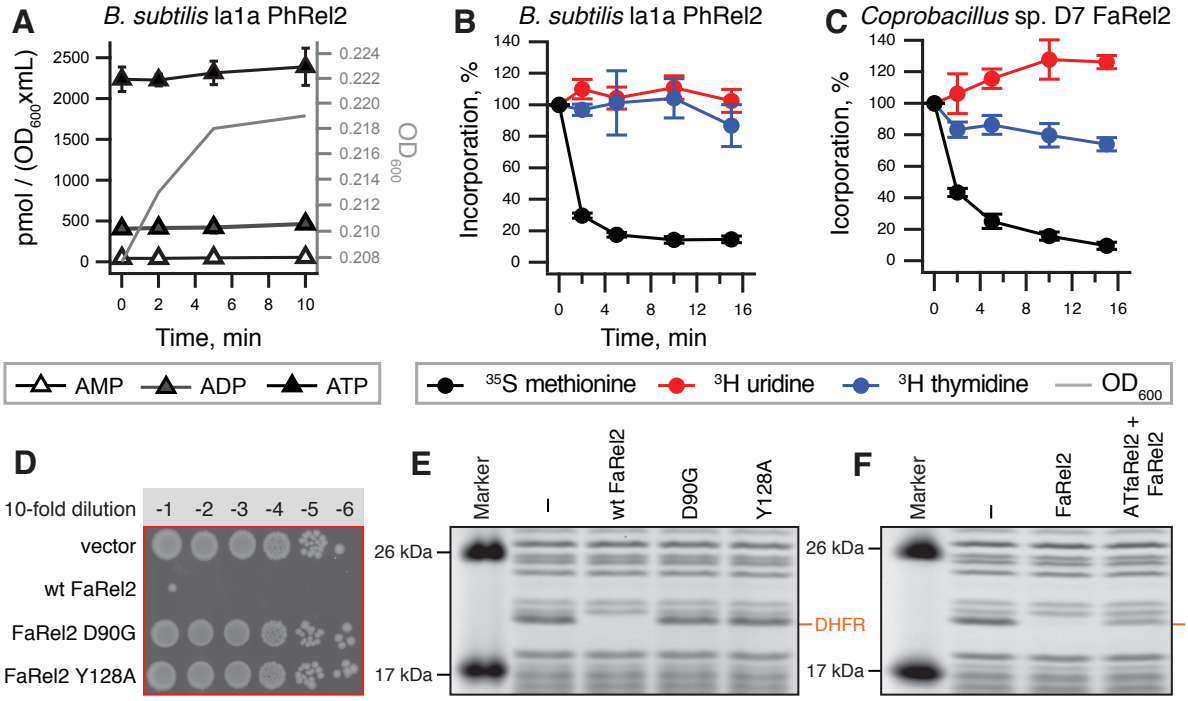

Figure 1. Inhibition of protein synthesis is an evolutionary widespread mechanism of toxSAS-mediated growth arrest.

(**A**) The expression of *B. subtilis* la1a PhRel2 does not perturb the adenosine nucleotide pools and (pp)pApp is not detectable upon expression of the toxin. Analogous experiments with *C. marina* FaRel and *Coprobacillus* sp. D7 FaRel2 are presented in **Figure S1**.

(**B, C**) Pulse-labelling assays following incorporation of ^{35}S-methionine (black traces), ^{3}H-uridine (red traces) and ^{3}H-thymidine (blue traces). The expression of *B. subtilis* la1a PhRel2 (**B**) and *Coprobacillus* sp. D7 FaRel2 (**C**) from the pBAD33-based constructs was induced with 0.2% L-arabinose. Analogous experiments with *P. aeruginosa* Tas1, *Mycobacterium* phage Phrann PhRel (Gp29) and *M. tuberculosis* AB308 CapRel toxSAS are presented in **Figure S3**.

(**D**) D90G and Y128A substitutions render FaRel2 non-toxic.

(**E, F**) Cell-free expression assays. Wild-type but not D90G or Y128A substituted FaRel2 abrogates production of DHFR (**E**). The addition of the ATfaRel2 antitoxin counteracts the inhibitory effect of FaRel2 (**F**).

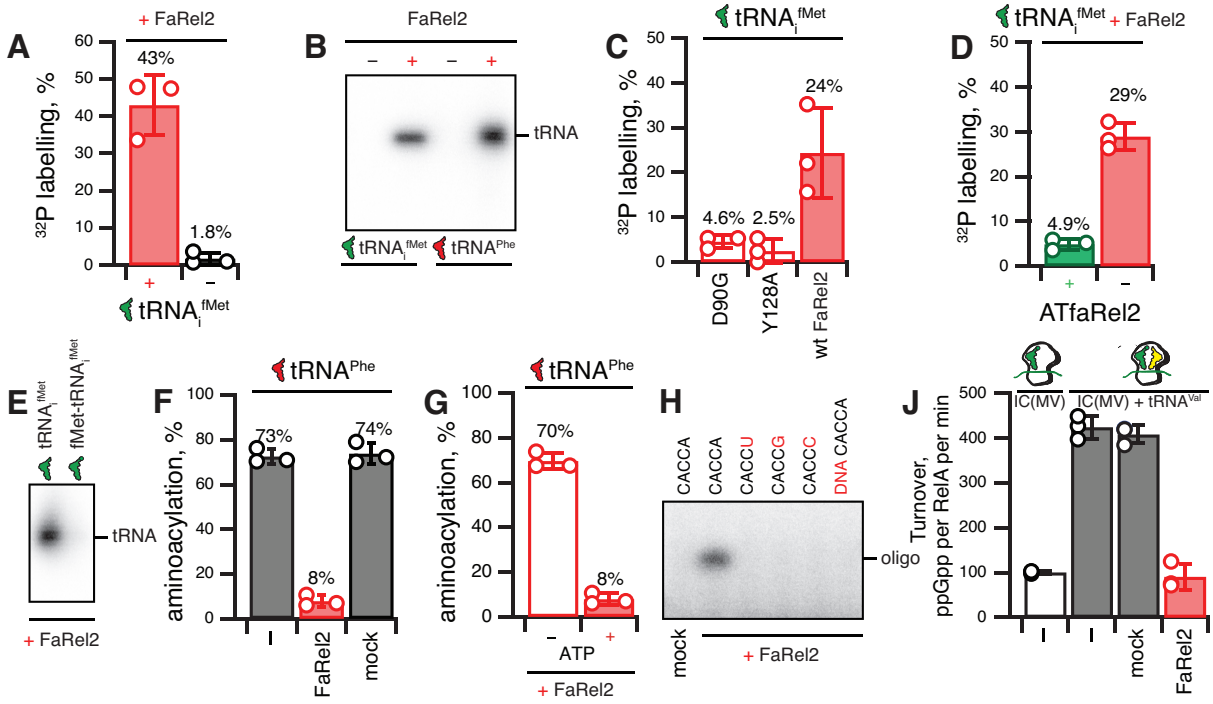

Figure 2. The FaRel2 toxSAS toxin modifies the 3′ CCA end of tRNA to inhibit aminoacylation and the sensing of amino acid starvation by RelA.

(**A, B**) A reconstituted ^{32}P transfer reaction using FaRel2 and either $tRNA_i^{fMet}$ or $tRNA^{Phe}$ as a substrate.

(**C**) Non-toxic D90G and Y128A FaRel2 mutants are compromised in their ability to modify tRNA.

(**D**) The ATfaRel2 antitoxin counteracts tRNA modification by FaRel2.

(**E**) Acylated fMet-$tRNA_i^{fMet}$ is refractory to modification by FaRel2.

(**F**) $tRNA^{Phe}$ modification by FaRel2 inhibits aminoacylation. As specificity controls, the reactions were supplemented either with mock protein preparation from *E. coli* strain transformed with an empty plasmid vector (mock) or HEPES:Polymix buffer (–).

(**G**) Inhibition of $tRNA^{Phe}$ aminoacylation by FaRel2 is strictly ATP-dependent.

(**H**) 3′ adenosine defines the specificity of modification by FaRel2, as tested using a set of model 5′-CACCN-3′ RNA oligonucleotides. 5′-CACCA-3′ DNA does not serve as a substrate for FaRel2.

(**J**) FaRel2 abrogates the stimulatory effect of deacylated $tRNA^{Val}$ on ppGpp synthesis by *E. coli* RelA in the presence of 70S ribosomal initiation complexes. Error bars represent standard deviations of the mean. The mock sample was produced by immunoprecipitation using *E. coli* cells transformed with a plasmid vector not expressing $FLAG_3$-tagged FaRel2.

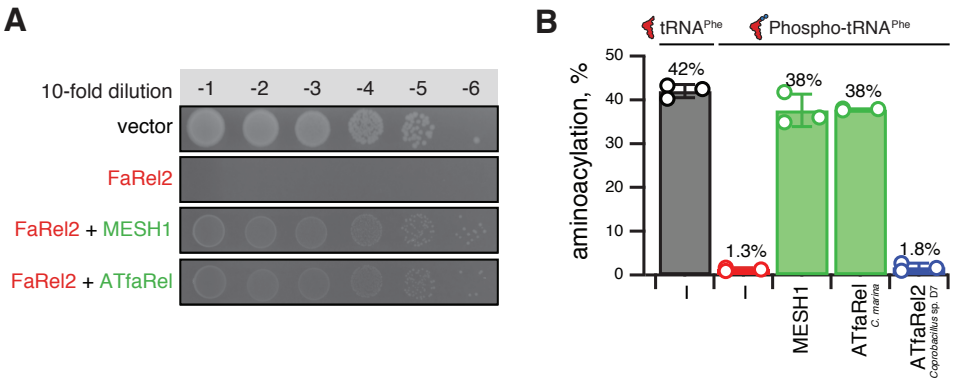

Figure 3. *C. marina* ATfaRel and MESH1 SAH enzymes detoxify FaRel2 through restoration of tRNA aminoacylation.

(**A**) Co-expression of human MESH1 and *C. marina* ATfaRel SAH enzymes counteracts the toxicity of *Coprobacillus* sp. D7 FaRel2 toxSAS. The SAH enzymes and FaRel2 toxSAS were induced and expressed from different plasmids, pMG25 and pMR33 derivatives respectively. (**B**) SAH enzymes MESH1 and ATfaRel but not cognate ATfaRel2 Type II antitoxin restore aminoacylation of $tRNA^{Phe}$ abrogated by FaRel2 by CCA pyrophosphorylation. As specificity controls the reactions were supplemented with HEPES:Polymix buffer (–).

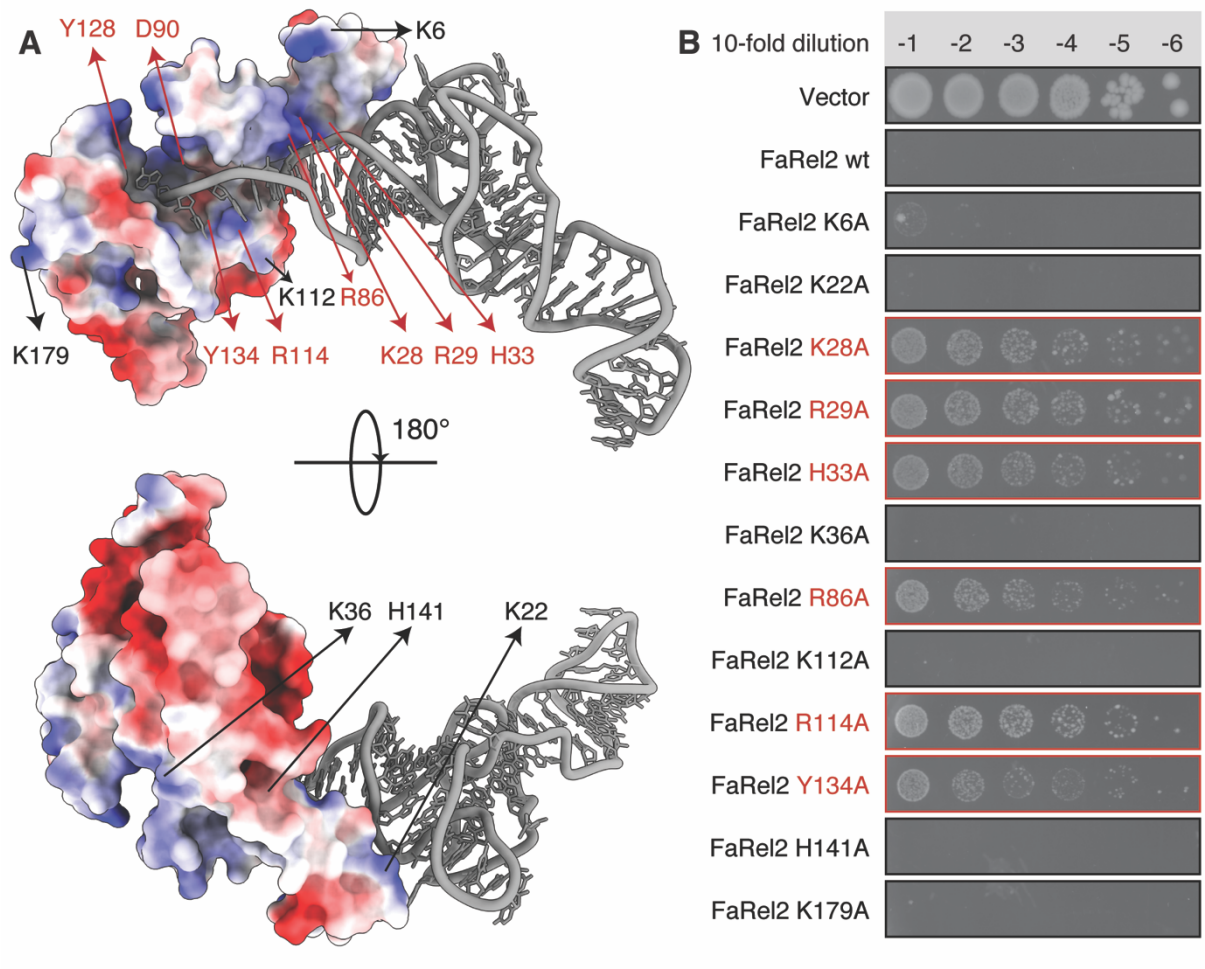

Figure 4. Mutational mapping of the predicted FaRel2: 3′ CCA tRNA interface.
(**A**) Surface representation of the model of the FaRel2:tRNA^{Phe} complex. The surface is colored on the basis of electrostatic potential. The phosphodiester backbone of the bound tRNA^{Phe} complements a cluster of positive charges at the active site exit of the enzyme. The predicted FaRel2:tRNA^{Phe} interface involves residues K28, R29, H33, R86, R114 and Y134. While these which guide the CCA end into the active site, functionally essential residue Y128 coordinates the 3′ adenosine of the CCA.
(**B**) Ten-fold dilutions of overnight cultures of *E. coli* strains transformed with the pBAD33 vector plasmid or derivatives expressing either wild-type *faRel2* or FaRel2 variants with Ala substitutions at the predicted tRNA-binding interface (K28, R29, H33, R86, R114 and Y134), neighbouring residues (K6, K22, K112 and H141), and positively charged residues outside the binding region (H36 and K179). The latter were served as negative controls. Substitutions at predicted tRNA-binding interface specifically abrogate toxicity of FaRel2.

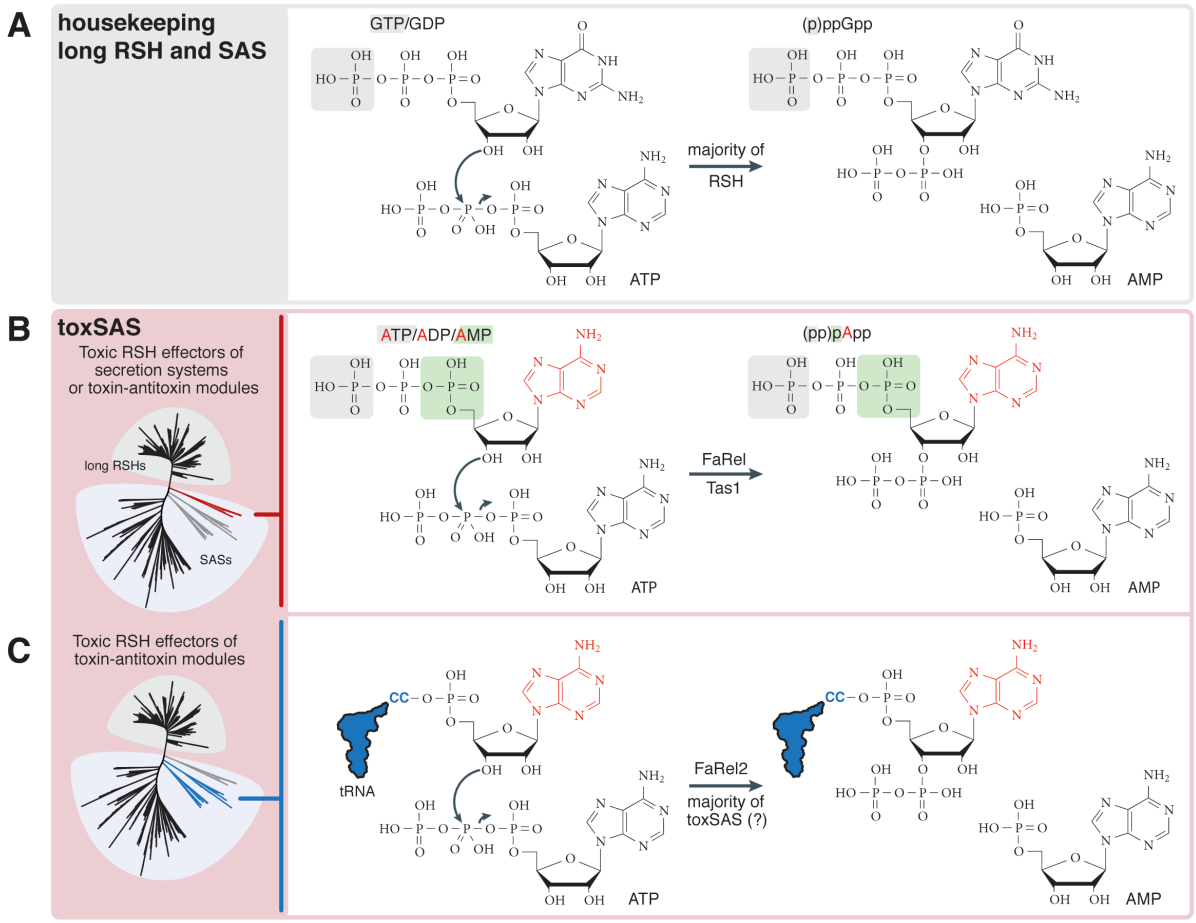

Figure 5. RSH differences in substrate specificity, from nucleotide-mediated signalling via production of (p)ppGpp and (pp)pApp alarmones to toxic modification of the tRNA 3′ CCA end.

(**A**) Housekeeping RSHs synthesise (p)ppGpp by transferring the pyrophosphate group of ATP onto the 3′ ribose position of either GDP or GTP, and degrade the alarmone by hydrolysing the nucleotide back to GDP or GTP.

(**B**) The substrate specificity of the Tas1 toxic SAS secretion system effectors and FaRel toxic components of toxin-antitoxin systems deviate from strict recognition of the guanine moiety of GDP/GTP employed by 'housekeeping' RSHs in favour of the adenine moiety of ATP/ADT/AMP to produce toxic (pp)pApp alarmones.

(**C**) The majority of identified toxSAS subfamilies specifically inhibit protein synthesis. FaRel2 toxic components of toxin-antitoxin systems recognise the adenine moiety of tRNA 3′ CCA instead of ATP/ADT/AMP nucleotides, and transfer the pyrophosphate group of ATP onto the 3′ ribose position tRNA 3′ terminal adenosine. This modification abrogates both tRNA aminoacylation and recognition by the amino acid sensor RSH RelA.

SUPPLEMENTAL FIGURES AND TABLES

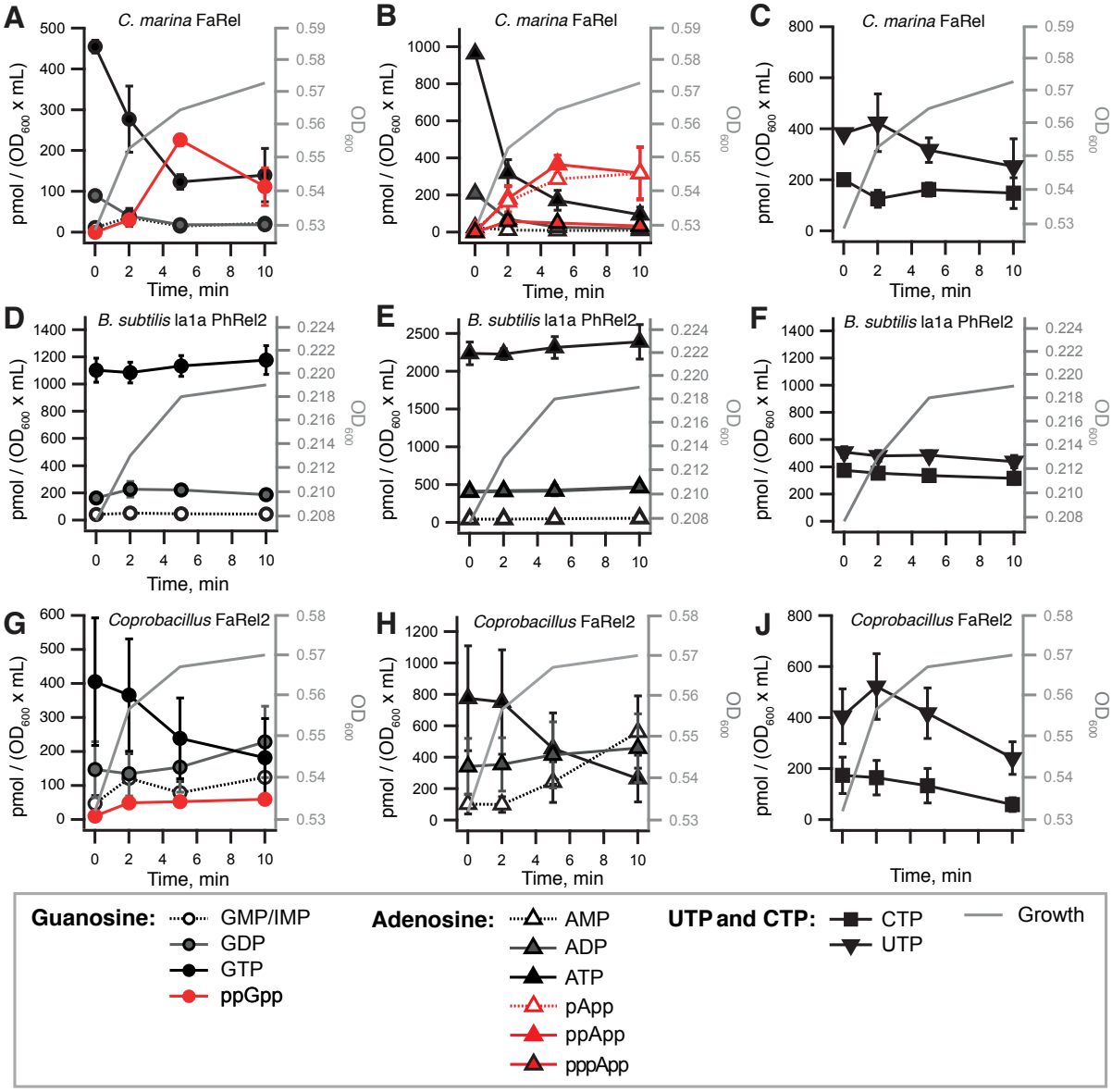

Figure S1. Nucleotide pools in *E. coli* BW25113 expressing *C. marina* FaRel, *B. subtilis* la1a PhRel2 and *Coprobacillus* sp. D7 FaRel2, related to Figure 1.

Cell cultures were grown in defined minimal MOPS medium supplemented with 0.5% glycerol at 37 °C with vigorous aeration. The expression of toxic SAS RSHs was induced with 0.2% L-arabinose at the OD_{600} 0.5 (FaRel and FaRel2) or 0.2 (PhRel2). Intracellular nucleotides are expressed in pmol per OD_{600} • mL as per the insert. Error bars indicate the standard error of the arithmetic mean of biological replicates.

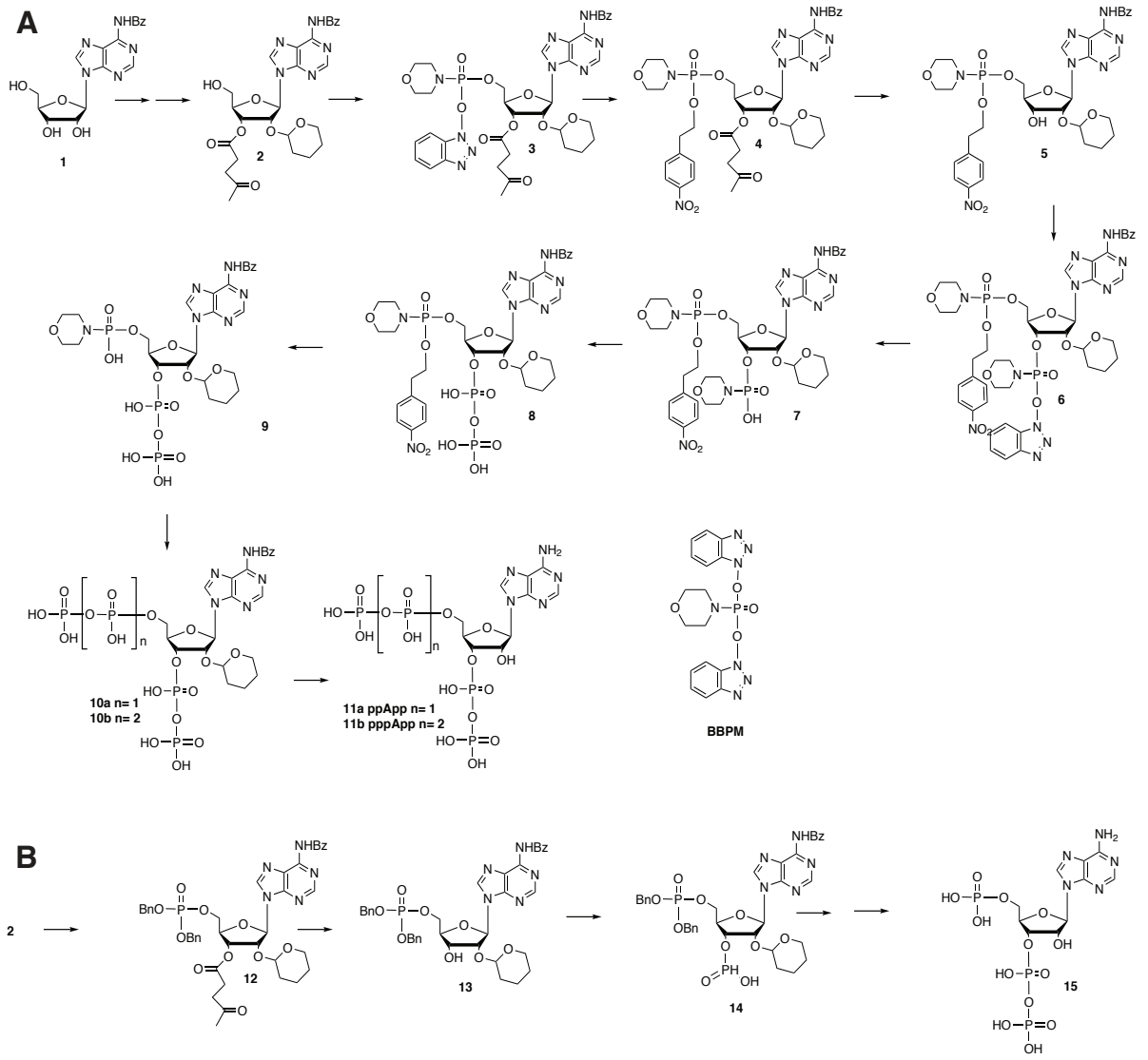

Figure S2. Synthesis of pppApp, ppApp and pApp, related to Figure 1.

(**A**) Synthesis of ppApp and pppApp. N^6-benzoyl adenosine (**1**) was used as a key starting material. Protected adenosine **2** reacted with reagent **BBPM** (bis(benzotriazolyl)phosphomorpholidate, see instert) affording intermediate **3**. Benzotriazolyl group of **3** was exchanged for 4-nitrophenylethyl group yielding **4**. Next, the 3′-levulinyl protecting group was removed (hydrazine, AcOH, pyridine). The resultant intermediate **5** was reacted again with BBPM affording **6**. Hydrolysis of benzotriazolyl group (Et_3N, H_2O, MeCN) provided morpholidate **7** that reacted with tributylamonium salt of phosphoric acid yielding 3′-diphosphate **8**. Removal of 4-nitrophenylethyl group (DBU, MeCN) afforded 5′-morpholidate **9** that upon reaction with tributylamonium salt of phosphoric or pyrophosphoric acid formed protected tetra- **10a** or pentaphosphate **10b**. The final products, ppApp (**11a**) and ppApp (**11b**), were obtained by removal of remaining protecting groups. Importantly, benzoyl group should be removed from nucleobase by treatment with aqueous ammonia first followed by removal of the THP group with 0.1N HCl (to avoid a nucleophilic attack of 2′-hydroxyl oxygen atom on phosphorus atom of 3′-phosphate moiety).

(**B**) Synthesis of pApp. Dibenzyl phosphate was installed to 5′-position of protected adenosine **2** by reaction with dibenzyl diisopropylphosphoramidite under tetrazole catalysis followed by oxidation with 4-chloroperbenzoic acid affording **12**. Removal of levulinyl protecting group

459 with hydrazine afforded intermediate **13** that was finally converted to pApp **14** using the same
460 methodology as for the synthesis of ppApp.
461

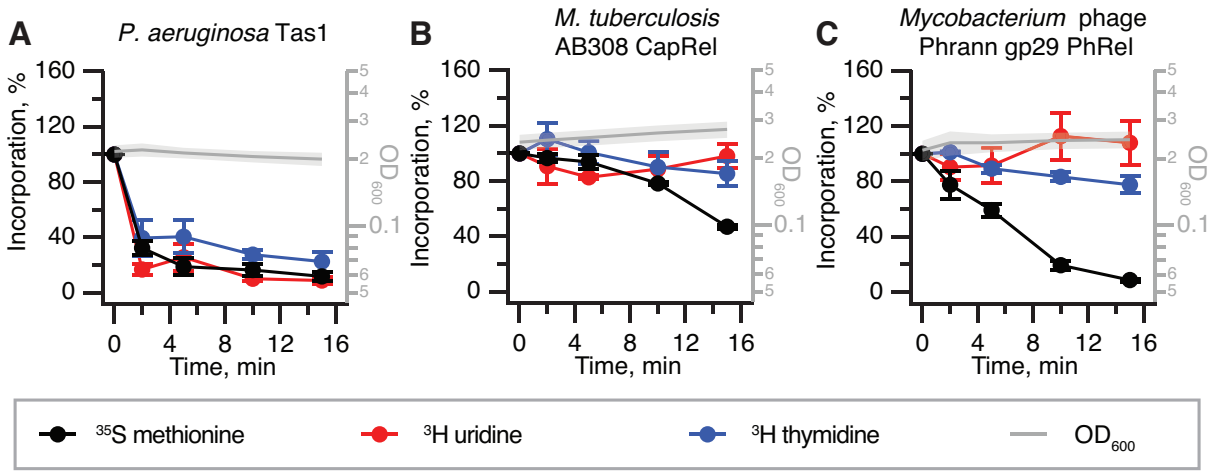

Figure S3. While expression of the (pp)pApp-synthesising *P. aeruginosa* Tas1 secretion system effector results in inhibition of transcription, translation and replication, the expression of *M. tuberculosis* AB308 CapRel or *Mycobacterium* phage Phrann PhRel toxSAS leads to specific inhibition of translation, related to Figure 1.

Pulse-labelling assays following incorporation of ^{35}S-methionine (black traces), ^{3}H-uridine (red traces), and ^{3}H-thymidine (blue traces). Expression of *P. aeruginosa* Tas1 (**B**), *M. tuberculosis* AB308 CapRel (**A**) or *Mycobacterium* phage Phrann PhRel (Gp29) (**c**) from the pBAD33-based constructs was induced by the addition of L-arabinose (final concentration 0.2%) to bacterial cultures in early exponential phase.

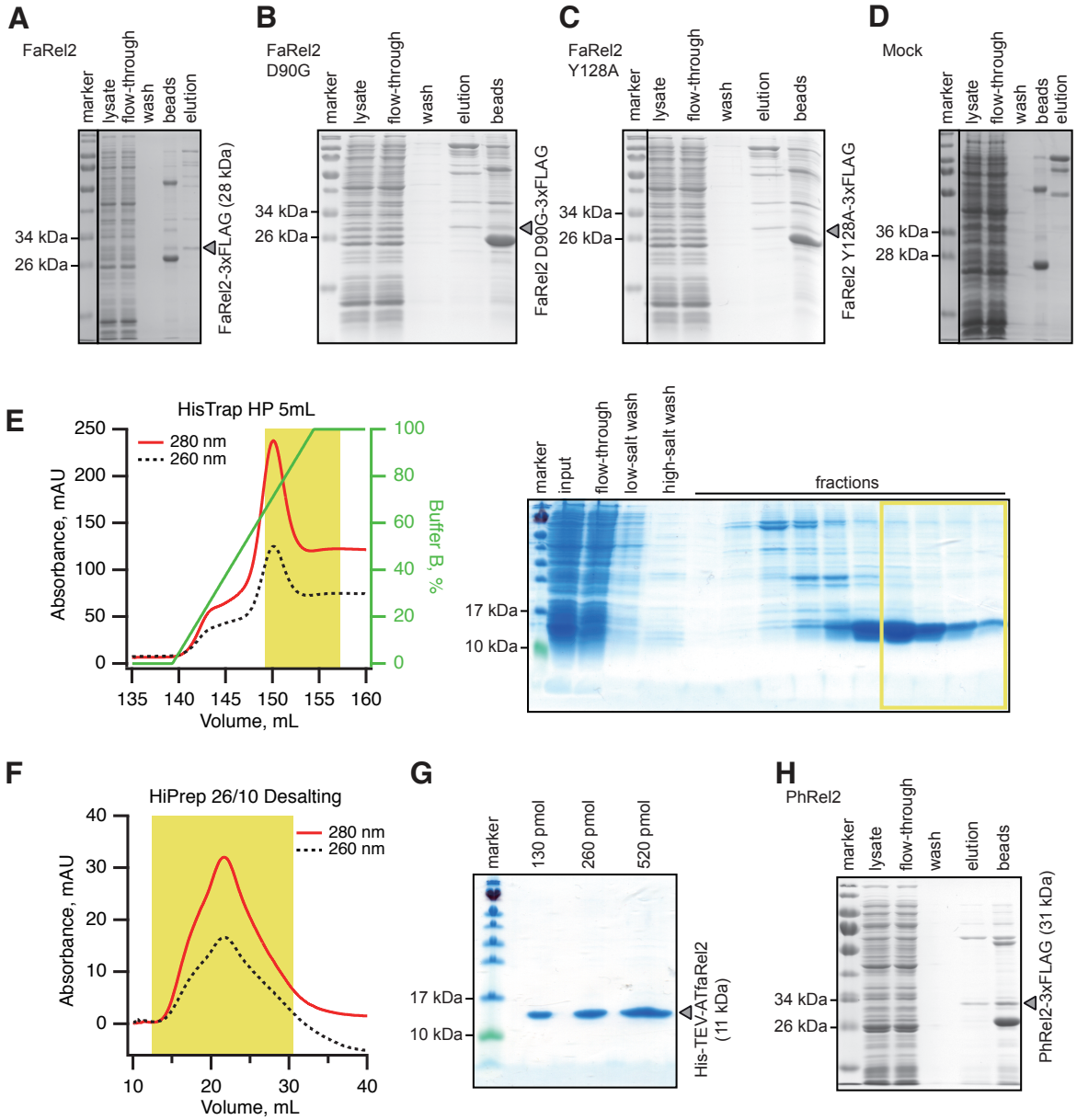

Figure S4. Protein purification of the FaRel2 toxSAS variants (A-D), ATfaRel2 antitoxin (E-G) and PhRel2 toxSAS, related to Figures 1, 2, 3 and S6.

FLAG$_3$-taged FaRel2 (**A**), FaRel2 D90A (**B**) and FaRel2 Y128A (**C**) proteins were immunoprecipitated with the anti-FLAG antibody and eluted with FLAG$_3$ peptide.

(**D**) Mock sample preparation from *E. coli* transformed with an empty vector (pBAD33) followed the same procedure as for toxin purification. Samples in each step were resolved by SDS-PAGE and visualised by Blue silver staining.

(**E**) Cells expressing N-terminally His$_6$-TEV-tagged ATfaRel2 were lysed and subjected to immobilised metal affinity chromatography (IMAC) using a HisTrap 5 mL HP column. The fraction corresponding to ATfaRel2 with the lowest contamination of other proteins (highlighted in yellow) was carried forward. Following the buffer exchange on HiPrep 10/26 desalting column (**F**), the fractions highlighted in yellow were pooled, concentrated, aliquoted, flash-frozen in liquid nitrogen and stored at –80 °C.

(**G**) SDS-PAGE analysis of the purified ATfaRel2.

(**H**) FLAG$_3$-taged PhRel protein was immunoprecipitated with the anti-FLAG antibody and eluted with FLAG$_3$ peptide.

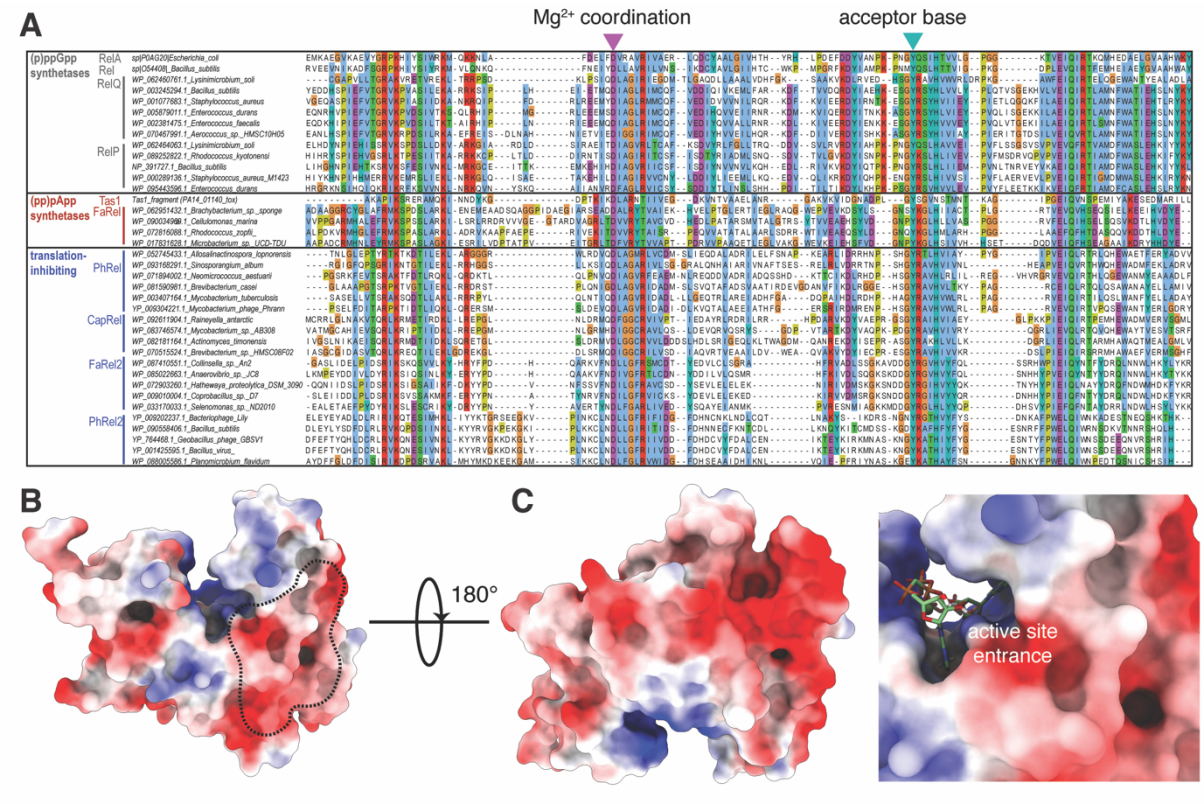

Figure S5. Sequence and structure of RSH SYNTH active sites, related to Figure 4.

(**A**) Sequence alignment of the SYNTH domain of selected RSHs. Sequences are divided into groups based on their functional capabilities (left panel). Invariant functionally important positions that are substituted in *Coprobacillus* sp. D7 FaRel2 are indicated with triangles (D90A and Y128A shown in purple and turquoise respectively).

(**B**) Surface charge distribution of *Staphylococcus aureus* RelQ (PDBID 6EWZ), the region equivalent to the tRNA-binding interface discovered in FaRel2 (highlighted in black) is highly negatively charged and likely precludes tRNA binding.

(**C**) ATP and GDP binding sites are positively charged to stabilize the poly-phosphate groups of ATP and GDP/GTP.

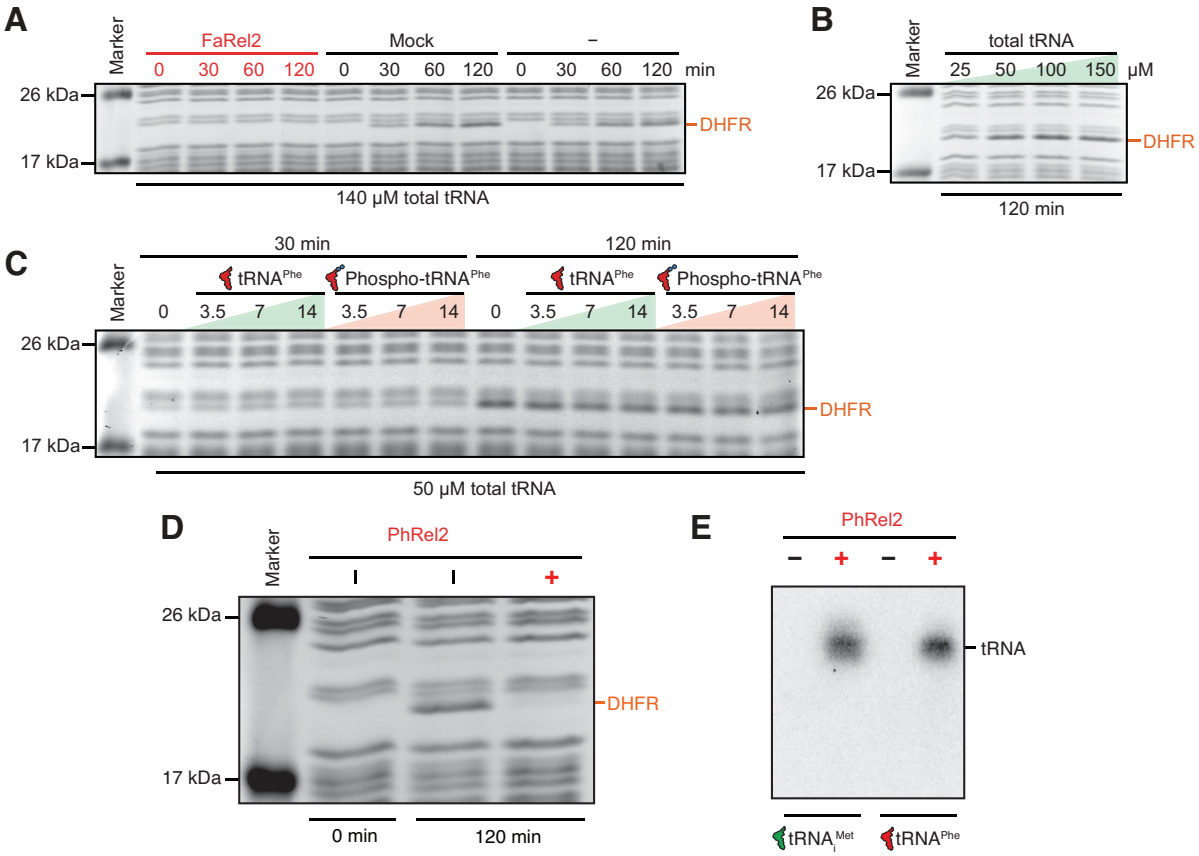

Figure S6. tRNA^{Phe} phosphorylated by FaRel2 does not inhibit translation in PURE system, related to Figures 1 and 2.

(**A**) The cell-free protein synthesis reactions were supplemented with same volume of either 50 nM FaRel2-FLAG$_3$ purified from *E. coli* FaRel2-FLAG$_3$ expressing strain (FaRel2), mock protein preparation from *E. coli* strain transformed with an empty plasmid vector (mock) or HEPES:Polymix buffer pH 7.5 (–).

(**B**) The concentration of total *E. coli* tRNA was titrated in PURE system and DHFR production was assessed by SDS PAGE at 120 minutes.

(**C**) Phosphorylated elongator tRNA^{Phe} titrated into the PURE system containing 50 µM total tRNA. Cell-free synthesis reactions were performed at 37 °C, the duration of the reaction is indicated on the individual panels.

(**D**) Addition of *B. subtilis* la1a PhRel2-FLAG$_3$ abrogates production of DHFR in cell-free expression assays.

(**E**) A reconstituted ^{32}P transfer reaction using PhRel2and either tRNA$_i^{fMet}$ or tRNA^{Phe} as a substrate.

520 **Table S1. Strains, plasmids and oligonucleotide primers used in this study.**

521

Strain	Name	Description	Reference/source
E. coli BL21 DE3	B F– *ompT gal dcm lon hsdS$_B$*(r_B– m_B–) λ(DE3 [*lacI lacUV5-T7p07 ind1 sam7 nin5*]) [*malB*$^+$]$_{K-12}$(λ^S)	*E. coli* strain used for pull-down assays	Laboratory stock
E. coli BW25113	F-, Δ(*araD-araB*)*567*, Δ*lacZ4787*(::rrnB-3), *λ-*, *rph-1*, Δ(*rhaD-rha*B)*568*, *hsdR514*	wild-type *E. coli* BW25113	(Grenier et al., 2014)
E. coli VHB15	*Nals strs rifs thi- lac- ara- gal+ mtl- F- recA+ uvr+ ion+ [pREP4 KanR]*	*E. coli* M15 (pREP4) used for PheRS purification	Qiagen
E. coli MC1061	*K-12 F– λ– Δ(ara-leu)7697 [araD139]B/r Δ(codB-lacI)3 galK16 galE15 e14– mcrA0 relA1 rpsL150(StrR) spoT1 mcrB1 hsdR2(r–m+)*	*E. coli* strain used for cloning and toxicity assay	Laboratory stock
Plasmid	**Name**	**Description**	**Reference/source**
pBAD33	pBAD33	p15A, Cml^R, P_{BAD} promoter	(Guzman et al., 1995)
pMR33	pMR33	p15A, Kan^R, P_{BAD} promoter	This work
pKK223-3	pKK223-3	ColE1, Amp^R, P_{Tac} promoter	(Brosius and Holy, 1984)
pET24d	pET24d	ColE1, Kan^R, T7 promoter, N-terminal T7-tag, C-terminal His_6-tag	Novagen
pMG25	pMG25	pUC *lacIq* $P_{A1/04/03}$ promoter, Amp^R	PMID: 25491382
VHp30	pPheRS	C-terminally His_6-tagged *E. coli* phenylalanyl-tRNA synthetase expressed under the control of T5 promoter and *lac* operator.	Gift from Måns Ehrenberg
VHp220	pBAD33-*phRel* (Phrann)	PhRel toxin from *Mycobacterium* Phage Phrann expressed under the control of P_{BAD} promoter	(Jimmy et al., 2020)
VHp277	pBAD33-*faRel2*	FaRel2 toxin expressed under the control of P_{BAD} promoter	(Jimmy et al., 2020)

VHp303	pBAD33-*phRel2*	PhRel2 toxin expressed under the control of P_{BAD} promoter	(Jimmy et al., 2020)
VHp313	pET24d-his6-aTfaRel	N-terminally His_6-tagged aTfaRel antitoxin expressed under the control of T7 promoter	This work
VHp364	pET24d-*6xhis-TEV-aTfaRel2*	N-terminally His_6-TEV-tagged aTfaRel2 antitoxin expressed under the control of T7 promoter	(Jimmy et al., 2020)
VHp366	pBAD33-*faRel2 Y128A*	Y128A FaRel2 toxin expressed under the control of P_{BAD} promoter; strong Shine-Dalgarno sequence	(Jimmy et al., 2020)
VHp380	pBAD33-*capRel* SD_{strong}	CapRel toxin expressed under the control of P_{BAD} promoter	(Jimmy et al., 2020)
VHp484	pBAD33-*his10-SUMO-faRel Y175A* SD_{strong}	N-terminally His_{10}-SUMO-tagged Y175A FaRel toxin expressed under the control of P_{BAD} promoter; strong Shine-Dalgarno sequence	(Jimmy et al., 2020)
VHp487	pET21b-*his6-TEV*-MESH1	N-terminally His_6-TEV-tagged MESH1 antitoxin expressed under the control of T7 promoter	This work
VHp678	pBAD33-*faRel2-3xFLAG* SD_{strong}	C-terminally $FLAG_3$-tagged FaRel2 toxin expressed under the control of P_{BAD} promoter; strong Shine-Dalgarno sequence	(Jimmy et al., 2020)
VHp679	pBAD33-*faRel2-3xFLAG Y128A* SD_{strong}	C-terminally $FLAG_3$-tagged Y128A FaRel2 toxin expressed under the control of P_{BAD} promoter; strong Shine-Dalgarno sequence	This work
VHp701	pET24d-*aTfaRel*	aTfaRel antitoxin expressed under the control of T7 promoter	This work
VHp770	pBAD33-*faRel2 D90G*	D90G FaRel2 toxin expressed under the control of P_{BAD} promoter	This work
VHp771	pBAD33-*faRel2-3xFLAG D90G* SD_{strong}	C-terminally $FLAG_3$-tagged D90G FaRel2 toxin expressed under the control of under	This work

		control of P_{BAD} promoter; strong Shine-Dalgarno sequence	
	pMG25-MESH1	ATfaRel SAH from human expressed under the control of $P_{A1/04/03}$ promoter	This work
	pMG25-*ATfaRel*	ATfaRel SAH from *Cellulomonas marina* expressed under the control of $P_{A1/04/03}$ promoter	This work
VHp816	pMR33-*faRel2*	FaRel2 toxin expressed under the control of P_{BAD} promoter	This work
VHp818	pMR33-*faRel*	FaRel toxin expressed under the control of P_{BAD} promoter	This work
VHp847	pMG25-*paSpo*	PaSpo SAH from *Salmonella* phage SSU5 expressed under the control of $P_{A1/04/03}$ promoter	This work
VHp930	pBAD33-*faRel2 K6A*	K6A FaRel2 toxin expressed under the control of P_{BAD} promoter	This work
VHp931	pBAD33-*faRel2 K22A*	K22A FaRel2 toxin expressed under the control of P_{BAD} promoter	This work
VHp932	pBAD33-*faRel2 K28A*	K28A FaRel2 toxin expressed under the control of P_{BAD} promoter	This work
VHp933	pBAD33-*faRel2 R29A*	R29A FaRel2 toxin expressed under the control of P_{BAD} promoter	This work
VHp934	pBAD33-*faRel2 H33A*	H33A FaRel2 toxin expressed under the control of P_{BAD} promoter	This work
VHp935	pBAD33-*faRel2 K36A*	K36A FaRel2 toxin expressed under the control of P_{BAD} promoter	This work
VHp936	pBAD33-*faRel2 R86A*	R86A FaRel2 toxin expressed under the control of P_{BAD} promoter	This work
VHp937	pBAD33-*faRel2 K112A*	K112A FaRel2 toxin expressed under the control of P_{BAD} promoter	This work

VHp938	pBAD33-*faRel2 R114A*	R114A FaRel2 toxin expressed under the control of P_{BAD} promoter	This work
VHp939	pBAD33-*faRel2 Y134A*	Y134A FaRel2 toxin expressed under the control of P_{BAD} promoter	This work
VHp940	pBAD33-*faRel2 H141A*	H141A FaRel2 toxin expressed under the control of P_{BAD} promoter	This work
VHp941	pBAD33-*faRel2 K179A*	K179A FaRel2 toxin expressed under the control of P_{BAD} promoter	This work
Oligo	**Sequence, 5′ to 3′**		**Reference/source**
VTK19	GAGCTCGAATTCGCTAGC		Metabion
VTK24	CGTTCTGATTTAATCTGTATCAGG		Metabion
VTK43	GGCGGCGACTACAAAGACC		Metabion
VTK45	TGGTCTTTGTAGTCGCCGCCAATTTTCTTGCAGTGATACAGCACATC		Metabion
VTK51	GGGCTAGCGAATTCGAGCTCAGGAGGAATTAAATGTACATCCTGGATAAGATTGGCCTTAAC		Metabion
VTK63	CACCACCACTGAGATCCGGC		Metabion
VTK69	GGGCTAGCGAATTCGAGCTC		Metabion
VTK80	GGGCTAGCGAATTCGAGCTC		Metabion
VTK81	GGTATATCTCCTTCTTAAAGTTAAACAAAATTATTTC		Metabion
VTK83	GCCGGATCTCAGTGGTGGTGCTTCTCTCATCCGCCAAAACAG		Metabion
VTK132	GTGTCTTTAACGGCATTCTGGGTTTTC		Metabion
VTK133	GAAAACCCAGAATGCCGTTAAAGACAC		Metabion
faRel2 K6A For	GCGATTGGCCTTAACATTGAGATTCTG		Sigma
faRel2 K6 Rev	ATCCAGGATGTACATGAGCTC		Sigma
faRel2 K22A For	GCGCTGGGAATGTCGTTTAAACGC		Sigma
faRel2 K22 Rev	CGATTCGTAGCTCAAGCTC		Sigma
faRel2 K28A For	GCGCGCACTCTGAGTCACTTC		Sigma
faRel2 K28-29 Rev	AAACGACATTCCCAGTTTCG		Sigma
faRel2 R29A For	AAAGCGACTCTGAGTCACTTCAACAAAGAG		Sigma
faRel2 H33A For	GCGTTCAACAAAGAGGAAGTGTTGAAAG		Sigma

faRel2 H33 Rev	ACTCAGAGTGCGTTTAAACGAC	Sigma
faRel2 K36A For	GCGGAGGAAGTGTTGAAAGAAATCGAAC	Sigma
faRel2 K36 Rev	GTTGAAGTGACTCAGAGTGC	Sigma
faRel2 R86A For	GCGGTCTTTAACGACATTCTGGGTTTTC	Sigma
faRel2 R86 Rev	ATTGTACGTTGCATTCGGG	Sigma
faRel2 K112A For	GCGATTCGCGTAGTAGACATGTCAC	Sigma
faRel2 K112-4 Rev	GTCCTCTTTCTCTAACTCCAACAC	Sigma
faRel2 R114A For	AAAATTGCGGTAGTAGACATGTCACGTGGC	Sigma
faRel2 Y134A For	GCGTATCAGCGTGATAACCACCATTATC	Sigma
faRel2 Y134 Rev	GACATGAATACCACGATAGCC	Sigma
faRel2 H141A For	GCGTATCCGATTGAAATCCAGTTTAACAC	Sigma
faRel2 H141 Rev	GTGGTTATCACGCTGATAGTAGAC	Sigma
faRel2 K179A For	GCGTACTACGAAAATGGCAAGATCAAATC	Sigma
faRel2 K179 Rev	GCGTAAGAGCTGACCAC	Sigma

522

METHODS

Bacterial strains

Bacterial strains and plasmids as well as oligonucleotide primers used in the study are listed in **Table S1**.

Multiple sequence alignment

Sequences were sequences extracted from the RSH database (Jimmy et al., 2020), aligned with MAFFT v7.164b with the L-ins-i strategy (Katoh and Standley, 2013), and alignments were visualised with Jalview (Waterhouse et al., 2009).

Construction of plasmids

Oligonucleotides were synthesised by Metabion and Sigma. To construct the plasmids, DNA fragments were amplified by PCR and assembled by NEBuilder HiFi DNA Assembly Cloning Kit (NEB, E5520S).

To construct VHp770, DNA fragments were amplified by PCR using VHp277 as a template as well as sets of primers VTK69 and VTK133 or VTK19 and VTK132. To construct VHp701, VHp308(Jimmy et al., 2020) and pET24d were used as PCR templates with primer sets of VTK80 and VTK83 or VTK63 and VTK81 respectively. To generate VHp771, the DNA fragments were amplified by PCR using VHp678 as the template and sets of primers VTK69 and VTK133 or VTK19 and VTK132. To construct VHp679, VHp366 and VHp678 were used as PCR templates with primers VTK51 and VTK45 or VTK19 and VTK43, respectively. The identity of the constructed plasmids was confirmed through re-sequencing (LGC genomics).

VHp818 and VHp816 were constructed by sub-cloning *faRel* and *faRel2* from VHp307 (Jimmy et al., 2020) and VHp227(Jimmy et al., 2020), respectively, into pMR33 using the restriction enzymes SacI and HindIII. The constructed plasmids were validated through sequencing (LGC genomics). The point mutations to *faRel2* was done in the plasmid VHp277 background and introduced by amplifying the entire plasmid with divergent primers listed in **Table S1**. The forward primer introduced the desired amino-acid substitution in its unbound 5′ region. After PCR with Q5 polymerase (NEB), the product was treated with DpnI (NEB) to remove the template plasmid, purified trough a PCR purification column (Omega), phosphorylated with PNK (NEB) and ligated (NEB). The mixture was transformed into *E. coli* MC1061 and the resulting plasmids were verified by sequencing (Eurofins).

Synthesis and characterisation of (pp)pApp

The synthesis of (p)ppApp (**Figure S2A**) followed the same procedure as for the preparation of pppGpp (Schattenkerk et al., 1985) but instead protected guanosine, N^6-benzoyl adenosine (**1**) was used as the starting material. The final products ((p)ppApp, **11a** and **11b**) were purified by preparative reversed phase HPLC using linear gradient of methanol in 0.1M aqueous TEAB. Triethylammonium salt was converted to potassium salt by passing through small column with Dowex 50 in K^+ phase, lyophilised from water and characterised by NMR and HR-MS. The synthesis of ppApp (**Figure S2B**) has been described in (Jimmy et al., 2020).

The synthesis of pApp followed a slightly different path. Dibenzyl phosphate was installed to the 5′-position of the protected adenosine **2** by reaction with dibenzyl diisopropylphosphoramidite under tetrazol catalysis, followed by oxidation with 4-chloroperbenzoic acid. Removal of the levulinyl protecting group was followed by installation of 3′-pyrophosphate using the same methodology as for the synthesis of ppApp.

ppApp 11a (I76DR_242P1)

^{1}H NMR (500.2 MHz, D_2O, ref(*t*BuOH) = 1.24 ppm): 4.21 – 4.27 (m, 2H, H-5); 4.59 (p, 1H, $J_{4',3'} = J_{4',5'} = J_{H,P} = 2.9$, H-4′); 4.88 (ddd, 1H, $J_{2',1'} = 6.5$, $J_{2',3'} = 5.0$, $J_{H,P} = 1.3$, H-2′); 4.98 (ddd, 1H, $J_{H,P} = 8.3$, $J_{3',2'} = 5.0$, $J_{3',4'} = 2.9$, H-3′); 6.22 (d, 1H, $J_{1',2'} = 6.5$, H-1′); 8.28 (s, 1H, H-2); 8.57 (s, 1H, H-8).

^{13}C NMR (125.8 MHz, D_2O, ref(*t*BuOH) = 32.43 ppm): 67.93 (d, $J_{C,P} = 5.3$, CH_2-5′); 76.54 (d, $J_{C,P}$ =4.5, CH-2′); 77.75 (d, $J_{C,P} = 5.2$, CH-3′); 86.41 (dd, $J_{C,P} = 9.1$, 3.8, CH-4′); 89.37 (CH-1′); 121.50 (C-5); 142.82 (CH-8); 152.17 (C-4); 155.73 (CH-2); 158.50 (C-6).

^{31}P{ ^{1}H} NMR (202.5 MHz, D_2O): -10.43 (d, $J = 21.8$, P_α-3′); -10.33 (d, $J = 20.7$, P_α-5′); -8.20 (bd, $J = 20.7$, P_β-5′); -6.45 (bd, $J = 21.8$, P_β-3′).

IR ν_{max} (KBr) 3436 (vs, br), 3250 (m, br, sh), 3155 (m, br, sh), 1636 (m, br), 1578 (w, sh), 1475 (w, br, sh), 1337 (vw), 1301 (vw), 1220 (w, br), 1103 (w, br), 1074 (w, br), 972 (w, br), 921 (w, br), 797 (vw).

HR-MS(ESI$^-$) For $C_{10}H_{16}O16_6N_5P_4$ $(M-H)^-$ calcd 585.95480, found 585.95518.

pppApp 11b (I76DR_265P1)

^{1}H NMR (500.2 MHz, D_2O, ref(*t*BuOH) = 1.24 ppm): 4.25 (ddd, 1H, $J_{gem} = 11.7$, $J_{H,P} = 4.9$, $J_{5'b,4'} = 2.8$, H-5′a); 4.28 (ddd, 1H, $J_{gem} = 11.7$, $J_{H,P} = 5.7$, $J_{5'a,4'} = 2.8$, H-5′a); 4.65 (p, 1H, $J_{4',3'}$

= $J_{4',5'}$ = $J_{H,P}$ = 2.8, H-4′); 4.87 (ddd, 1H, $J_{2',1'}$ = 7.0, $J_{2',3'}$ = 5.2, $J_{H,P}$ = 1.3, H-2′); 4.96 (bm, 1H, H-3′); 6.19 (d, 1H, $J_{1',2'}$ = 7.0, H-1′); 8.27 (s, 1H, H-2); 8.56 (s, 1H, H-8).

^{13}C NMR (125.8 MHz, D_2O, ref(*t*BuOH) = 32.43 ppm): 68.38 (d, $J_{C,P}$ = 5.2, CH_2-5′); 76.66 (d, $J_{C,P}$ = 4.9, CH-2′); 78.21 (d, $J_{C,P}$ = 6.0, CH-3′); 86.45 (dd, $J_{C,P}$ = 8.7, 2.9, CH-4′); 89.08 (CH-1′); 121.48 (C-5); 142.81 (CH-8); 152.25 (C-4); 155.66 (CH-2); 158.45 (C-6).

^{31}P{ ^{1}H} NMR (202.5 MHz, D_2O): -22.14 (t, *J* = 19.1, P$_\beta$-5′); -10.83 (d, *J* = 20.6, P$_\alpha$-3′); -10.63 (d, *J* = 19.1, P$_\alpha$-5′); -9.65 (bd, *J* = 19.1, P$_\gamma$-5′); -8.63 (bd, *J* = 20.6, P$_\beta$-3′).

HR-MS(ESI$^-$) For $C_{10}H_{17}O_{19}N_5P_5$ $(M-H)^-$ calcd 665.92113, found 665.91960.

pApp (I76DR_215P1)

^{1}H NMR (500.2 MHz, D_2O, ref(*t*BuOH) = 1.24 ppm): 4.12 (ddd, 1H, J_{gem} = 11.8, $J_{H,P}$ = 4.6, $J_{5'b,4'}$ = 2.8, H-5′a); 4.16 (ddd, 1H, J_{gem} = 11.8, $J_{H,P}$ = 4.8, $J_{5'a,4'}$ = 2.8, H-5′a); 4.59 (dt, 1H, $J_{4',3'}$ = 3.2, $J_{4',5'}$ = 2.8, H-4′); 4.85 (ddd, 1H, $J_{2',1'}$ = 6.2, $J_{2',3'}$ = 5.1, $J_{H,P}$ = 1.3, H-2′); 4.96 (ddd, 1H, $J_{H,P}$ = 8.5, $J_{3',2'}$ = 5.1, $J_{3',4'}$ = 3.2, H-3′); 6.19 (d, 1H, $J_{1',2'}$ = 6.2, H-1′); 8.26 (s, 1H, H-2); 8.53 (s, 1H, H-8).

^{13}C NMR (125.8 MHz, D_2O, ref(*t*BuOH) = 32.43 ppm): 67.01 (d, $J_{C,P}$ = 4.7, CH_2-5′); 76.58 (d, $J_{C,P}$ =4.6, CH-2′); 77.57 (d, $J_{C,P}$ = 5.4, CH-3′); 86.34 (dd, $J_{C,P}$ = 8.9, 4.0, CH-4′); 89.55 (CH-1′); 121.53 (C-5); 142.82 (CH-8); 152.09 (C-4); 155.71 (CH-2); 158.49 (C-6).

^{31}P{^{1}H} NMR (202.5 MHz, D_2O): -10.69 (d, *J* = 21.1, P$_\alpha$-3′); -7.94 (d, *J* = 21.2, P$_\beta$-3′); 1.51 (s, P-5′).

HR-MS(ESI$^-$) For $C_{10}H_{15}O_{13}N_5P_3$ $(M-H)^-$ calcd 505.98847, found 505.98861.

HPLC-based nucleotide quantification

E. coli strain BW25113 (Grenier et al., 2014) was transformed with RSH-expressing plasmids (pMR33-faRel, pMR33-faRel2 or pBAD33-phRel2) as well as empty pKK223-3 vector. The starter cultures were pre-grown overnight at 37 °C with vigorous shaking (200 rpm) in Neidhardt MOPS minimal media (Neidhardt et al., 1974) supplemented with 1 µg/mL thiamine, 1% glucose, 100 µg/mL carbenicillin as well as either 20 µg/mL chloramphenicol (pBAD33--phRel2) or 25 µg/mL kanamycin (pMR33-faRel and pMR33-faRel2). The overnight cultures were diluted to OD_{600} 0.05 in 115 mL of pre-warmed medium MOPS supplemented with 0.5% glycerol as carbon source and grown until $OD_{600} \approx 0.5$ (pMR33-faRel and pMR33-faRel2) or $OD_{600} \approx 0.2$ (pBAD33-phRel2) at 37 °C, 200 rpm. At this point 0.2% arabinose was added to induce the expression of the toxin. 26 mL samples were collected for HPLC analyses at 0, 2, 5 and 10 minutes after the addition of arabinose and IPTG. Nucleotide extraction and HPLC

analyses were performed as described previously (Varik et al., 2017). The OD_{600} measurements were performed in parallel with collection of the samples for HPLC analyses.

Metabolic labelling with ^{35}S-methionine, ^{3}H-uridine or ^{3}H-thymidine

Overnight cultures in defined Neidhardt MOPS minimal media (Neidhardt et al., 1974) supplemented with 1% glucose, 0.1% casamino acids and as well as appropriate antibiotics were inoculated with single colonies of *E. coli* BW25113 cells freshly transformed with pBAD33-based plasmid for L-arabinose-inducible RSH expression as well as the empty pKK223-3 vector. After overnight incubation at 37 °C with shaking at 180 rpm, the cultures were diluted to an OD_{600} of 0.05 in 15 mL MOPS minimal media supplemented with 19 amino acids (25 µg/mL, final concentration) but lacking methionine, 0.5% glycerol, as well as appropriate antibiotics. The cultures were grown at 37 °C until an OD_{600} of 0.2-0.3 in a water bath with shaking (200 rpm), and expression of toxins was induced with 0.2% L-arabinose. For a zero-point 1 mL of culture was taken and mixed with either 4.35 µCi ^{35}S-methionine (Perkin Elmer), 0.65 µCi ^{3}H-uridine (Perkin Elmer) or 2 µCi ^{3}H-thymidine (Perkin Elmer) immediately before induction. Simultaneously, another 1 mL of culture was taken for OD_{600} measurements. Samples were collected at 2, 5, 10 and 15 minutes post-induction and processed as described above. The incorporation of radioisotopes was quenched 8 minutes after addition of the isotope, by the addition of 200 µL ice-cold 50% trichloroacetic acid (TCA). Samples were filtered through GF/C filters (Whatman) prewashed with 5% TCA, followed by washing twice with 5 mL of ice-cold TCA and, finally, twice with 5 mL of 95% EtOH. The filters were dried at least for two hours at room temperature and the radioactivity was quantified by scintillation using EcoLite Liquid Scintillation Cocktail scintillation cocktail (5 mL per vial, MP Biomedicals, 15 minutes shaking with filters prior to counting) using a TRI-CARB 4910TR 100 V scintillation counter (PerkinElmer).

Toxicity validation assays

The experiments were performed as described earlier (Jimmy et al., 2020). The assays were performed on LB medium (Lennox) plates (VWR). We used *E. coli* BW25113 strain co-transformed with two different plasmid systems for controllable expression of toxins and antitoxin.

First, we used a combination of pKK223-3 (medium copy number, ColE1 origin of replication, Amp^R, antitoxins expressed under the control of P_{Tac} promoter (Brosius and Holy, 1984)) and pBAD33 harbouring toxin genes (medium copy number, p15A origin of replication,

658 Cml^R, toxins expressed under the control of P_{BAD} promoter (Guzman et al., 1995)) (**Figure 1D**
659 and **Figure 4B**). The cells were grown in liquid LB medium (BD) supplemented with
660 100 µg/mL carbenicillin (AppliChem) and 20 µg/mL chloramphenicol (AppliChem), 30 mM
661 K_2HPO_4/KH_2PO_4 (pH 7.4) as well as 1% glucose (repression conditions). Serial ten-fold
662 dilutions were spotted (5 µl per spot) on solid LB plates containing carbenicillin and
663 chloramphenicol in addition to either 1% glucose (repressive conditions), or 0.2% arabinose
664 combined with 1 mM IPTG (induction conditions). Plates were scored after an overnight
665 incubation at 37 °C. Sequences were codon-optimised for expression in *E. coli.*
666 Second, we used pMG25 (high copy number, ColE1 origin of replication (pUC), Amp^R,
667 antitoxin expressed under the control of IPTG inducible $P_{A1/04/03}$ promoter (Jaskolska and
668 Gerdes, 2015)) and pBAD-based pMR33 (this work) harbouring toxin genes (medium copy
669 number, p15A origin of replication, Kan^R, toxins expressed under the control of P_{BAD} promoter)
670 (**Figure 3A**). The cells were grown in liquid LB medium (BD) supplemented with 0.2% glucose
671 (repression conditions), 100 µg/mL carbenicillin (AppliChem) and 50 µg/mL kanamycin
672 (AppliChem). Serial dilutions and spotting were performed as described above using solid LB
673 plates supplemented with 0.2% arabinose as well as 100 µg/mL carbenicillin (AppliChem) and
674 50 µg/mL kanamycin (AppliChem).
675
676 **Protein expression and purification**
677 The *Coprobacillus* sp. D7 C-terminally $FLAG_3$-tagged FaRel2 (FaRel2-$FLAG_3$) was
678 overexpressed in freshly transformed *E. coli* BL21 DE3 co-transformed with the VHp701
679 plasmid encoding the non-tagged SAH aTfaRel antitoxin under the pET promoter. Fresh
680 transformants were inoculated to a final OD_{600} of 0.04 in the LB medium (800 mL)
681 supplemented with 100 µg/mL kanamycin and 20 µg/mL chloramphenicol. The cultures were
682 grown at 37 °C until an OD_{600} of 0.3, the antitoxin was pre- induced with 0.1 mM IPTG (final
683 concentration) for one hour and the toxin was induced with 0.2% arabinose (final concentration)
684 for an additional one hour at 37 °C. The cells were collected by centrifugation (8,000 rpm, 10
685 minutes at 4 °C, JLA-10.500 Beckman Coulter rotor), dissolved in 4 mL of cell suspension
686 buffer (20 mM HEPES:KOH pH 7.5, 95 mM KCl, 5 mM NH_4Cl, 0.5 mM $CaCl_2$, 8 mM
687 putrescine, 1 mM spermidine, 5 mM $Mg(OAc)_2$, 1 mM DTT and cOmplete protease inhibitor
688 (Mini, EDTA-free from Roche)). The cell suspension was divided to 1 mL aliquots, and 200 µl
689 of pre-chilled zirconium beads (0.1 mm) were added in the aliquots. Cellular lysates were
690 prepared by a FastPrep homogeniser (MP Biomedicals) (four 20 seconds pulses at speed 4.5
691 mp per second with chilling on ice for 2 minutes between the cycles) and clarified by

centrifugation at 21,000 g for 20 minutes at 4 °C. The supernatant was carefully collected, avoiding the lipid layer and cellular pellet.

30 mg of total protein (as determined by Bradford assay) of each sample was mixed with 100 µL of ANTI-FLAG M2 Affinity Gel (Sigma-Aldrich) and mixed by rotation for 2 hours at 4 °C. The mixture was loaded on a Micro Bio-Spin Chromatography Column (Bio-Rad) and flow-through was collected. The gel in the column was washed five times with 1 mL of cell suspension buffer supplemented with 10% glycerol, and the fraction at final wash was collected. The gel was mixed with 300 µL of cell suspension buffer supplemented with 10% glycerol as well as 0.1 mg/mL Poly FLAG Peptide lyophilised powder (Biotool) in the column by rotation for 40 min at 4 °C. The elution fraction was passed through the column by spinning down, and was collected in Eppendorf tube. After this elution step, the gel was suspended with 1x sample buffer (50 mM Tris:HCl pH 6.8, 2% SDS, 0.01% bromophenol blue, 10% glycerol, 10 mM DTT and 2% beta-mercaptoethanol) and collected. 0.5 µL of cell lysate, 0.5 µL of flowthrough, 8 µL of wash, 8 µL of elution fractions and 10 µL of gel suspension were resolved on 15% SDS-PAGE gel.

The SDS-PAGE gel was fixed with fixing solution (50% ethanol and 2% phosphoric acid) for 5 min at room temperature, washed with water for 20 minutes at room temperature twice, and stained with "blue silver" solution(Candiano et al., 2004) (0.12% Brilliant Blue G250 (Sigma-Aldrich, 27815), 10% ammonium sulfate, 10% phosphoric acid, and 20% methanol) overnight at room temperature. After washing with water for 3 hours at room temperature, the gel was analysed on an ImageQuant LAS 4000 (GE Healthcare) imaging system (**Figure S4A,D**). The concentration of FaRel2-$FLAG_3$ was quantified on SDS-PAGE gels by ImageJ(Schneider et al., 2012) using pure ATfaRel2 as a standard.

For Western blotting, the proteins resolved by similar electrophoresis were transferred to 0.2 µm nitrocellulose membrane (BioTrace™ NT, Pall) using Trans-Blot® Turbo™ Transfer System (Bio-Rad). To detect $FLAG_3$-tagged protein, the membrane was blocked in PBS-T (1xPBS supplemented with 0.05% Tween-20) with 5% w/v nonfat dry milk at room temperature for one hour, and first antibody incubation was performed for overnight at 4 °C in PBS-T anti-Flag M2 (Sigma-Aldrich F1804, batch number #SLCD3524; 1:5000 dilution). After three 5-minute washes in fresh PBS-T, second antibody incubations were performed for one hour at room temperature in PBS-T with Goat anti-Mouse IgG-HRP (Agrisera AS11 1772, batch number #810-103-040; 1:4,000 dilution). Tagged-proteins were detected on an

ImageQuant LAS 4000 (GE Healthcare) imaging system using WesternBright Quantum HRP substrate (Advansta).

The C-terminally $FLAG_3$-tagged *B. subtilis* la1a PhRel2 (PhRel2-$FLAG_3$) was overexpressed in freshly transformed *E. coli* BW25113 co-transformed with the VHp847 plasmid encoding the PaSpo SAH antitoxin under the IPTG-inducible promoter ($P_{A1/04/03}$ promoter). Fresh transformants were inoculated to a final OD_{600} of 0.05 in the LB medium (800 mL) supplemented with 100 µg/mL carbenicillin, 20 µg/mL chloramphenicol and 50 µM IPTG. The cultures were grown at 37 °C until an OD_{600} of 0.5, the toxin was induced with 0.2% arabinose (final concentration) for an additional 3 hours at 37 °C. The cells were collected by centrifugation (8,000 rpm, 10 minutes at 4 °C, JLA-10.500 Beckman Coulter rotor), dissolved in 4 mL of cell suspension buffer (20 mM HEPES:KOH pH 7.5, 95 mM KCl, 5 mM NH_4Cl, 0.5 mM $CaCl_2$, 8 mM putrescine, 1 mM spermidine, 5 mM $Mg(OAc)_2$, 1 mM DTT, and cOmplete, Mini, EDTA-free (Roche)). The cell suspension was divided to 1 mL aliquots, and 200 µl of pre-chilled zirconium beads (0.1 mm) were added in the aliquots. Cellular lysates were prepared by a FastPrep homogeniser (MP Biomedicals) (four 20 seconds pulses at speed 4.5 mp per second with chilling on ice for 2 minutes between the cycles) and clarified by centrifugation at 21,000 g for 20 minutes at 4 °C. The supernatant was carefully collected, avoiding the lipid layer and cellular pellet.

30 mg of total protein (as determined by Bradford assay) of each sample was mixed with 100 µL of ANTI-FLAG M2 Affinity Gel (Sigma-Aldrich) and mixed by rotation for 2 hours at 4 °C. The mixture was loaded on a Micro Bio-Spin Chromatography Column (Bio-Rad) and flow-through was collected. The gel in the column was washed with 1 mL of cell suspension buffer including 1 M KCl five times and 1 mL of cell suspension buffer supplemented with 10% glycerol five times, and the fraction at final wash was collected. The gel was mixed with 300 µL of cell suspension buffer supplemented with 10% glycerol and 0.1 mg/mL Poly FLAG Peptide lyophilised powder (Biotool) in the column by rotation for 40 min at 4 °C. The elution fraction was passed through the column by spinning down, and was collected in Eppendorf tube. After this elution step, the gel was suspended with 1x sample buffer (50 mM Tris:HCl pH 6.8, 2% SDS, 0.01% bromophenol blue, 10% glycerol, 10 mM DTT and 2% beta-mercaptoethanol) and collected. 0.5 µL of cell lysate, 0.5 µL of flowthrough, 8 µL of wash, 8 µL of elution fractions and 10 µL of gel suspension were resolved on 10% SDS-PAGE gel.

Coprobacillus sp. D7 N-terminally His_6-TEV-tagged ATfaRel2 was overexpressed in freshly transformed *E. coli* BL21(DE3) with VHp364. Fresh transformants were inoculated to a final OD_{600} of 0.05 in the LB medium (800 mL) supplemented with 100 µg/mL kanamycin. The cultures were grown at 37 °C until an OD_{600} of 0.5, induced with 0.4 mM IPTG (final concentration) and grown for an additional one hour at 30 °C. The cells were harvested by centrifugation and resuspended in buffer A (300 mM NaCl, 10 mM imidazole, 10% glycerol, 4 mM β-mercaptoethanol, 25 mM HEPES:KOH pH 8.0) supplemented with 0.1 mM PMSF and 1 U/mL of DNase I, and lysed by one passage through a high-pressure cell disrupter (Stansted Fluid Power, 150 MPa). Cell debris was removed by centrifugation (25,000 rpm for 1 hour) and clarified lysate was taken for protein purification. Clarified cell lysate was filtered through a 0.22 µm syringe filter and loaded onto a HisTrap 5 mL HP column pre-equilibrated in buffer A. The column was washed with 5 column volumes (CV) of buffer A and following buffer B (1 M NaCl, 10 mM imidazole, 10% glycerol, 4 mM β-mercaptoethanol, 25 mM HEPES:KOH pH 8.0), and the protein was eluted using a linear gradient (3 CV with 0-100%) of buffer C (300 mM NaCl, 300 mM imidazole, 10% glycerol, 4mM β-mercaptoethanol, 25 mM HEPES:KOH pH 8.0). Fractions enriched in ATfaRel2 (≈60% buffer C) were pooled totaling approximately 8 mL (**Figure S4E**). The sample was applied on a HiPrep 10/26 desalting column (GE Healthcare) pre-equilibrated with storage buffer (buffer D; 300 mM KCl, 10% glycerol, 4 mM β-mercaptoethanol, 25 mM HEPES:KOH pH 8.0). The fractions containing ATfaRel2 were collected (about 8 mL in total, (**Figure S4F**) and concentrated on an Amicon Ultra (Millipore) centrifugal filter device with a 3 kDa cut-off. The purity of protein preparations was assessed by SDS-PAGE (**Figure S4G**). Protein preparations were aliquoted, frozen in liquid nitrogen and stored at –80 °C. Individual single-use aliquots were discarded after the experiment.

For purification of RelA *E. coli* BL21 DE3 harbouring pET24d:his10-SUMO-relA expression constructs were grown, induced, harvested and lysed as described earlier (Kudrin et al., 2018). Protein purification was performed as previously described (Turnbull et al., 2019).

C-terminally His_6-tagged *E. coli* phenylalanyl-tRNA synthetase (PheRS) was overexpressed in *E. coli* BL21 (DE3). Fresh transformants were used to inoculate 3 L cultures of LB medium supplemented with 100 µg/mL ampicillin. The cultures were grown at 37 °C until an OD_{600} of 0.5, protein expression was induced with 1 mM IPTG (final concentration) and then the cultures were grown overnight at 37 °C. The cells were harvested by centrifugation, resuspended in buffer E (150 mM NaCl, 5 mM $MgCl_2$, 20 mM imidazole, 1 mM β-mercaptoethanol, 20 mM

Tris:HCl pH 7.5) supplemented with 1 mM PMSF, and lysed by one passage through a high-pressure cell disrupter. Cell debris was removed by centrifugation and clarified lysate was taken for protein purification. Clarified cell lysate was filtered through a 0.22 µm syringe filter and loaded onto a HisTrap 5 mL HP column pre-equilibrated in buffer E. The column was washed with 20 column volumes (CV) of buffer F (1 M NaCl, 5 mM $MgCl_2$, 20 mM imidazole, 1 mM β-mercaptoethanol, 20 mM Tris:HCl pH 7.5) and following buffer E (5 CV), and the protein was eluted using a linear gradient (30 CV with 0-100%) of buffer G (150 mM NaCl, 5 mM $MgCl_2$, 500 mM imidazole, 1 mM β-mercaptoethanol, 20 mM Tris:HCl pH 7.5). Fractions enriched in PheRS (≈45% buffer G) were pooled. The sample was applied on a HiPrep 10/26 desalting column (GE Healthcare) pre-equilibrated with storage buffer (buffer H; 100 mM KCl, 2 mM $MgCl_2$, 10% glycerol, 6 mM β-mercaptoethanol, 20 mM Tris:HCl pH 7.5). The fractions containing PheRS were collected. The protein was aliquoted, aliquots plunge-frozen in liquid nitrogen and stored at –80 °C. Individual single-use aliquots were discarded after the experiment.

Human MESH1 (VHp487, pET21b-His6-TEV-MESH1) was overexpressed in freshly transformed *E. coli* BL21 DE3 Rosetta (Novagen). Transformants were inoculated to a final OD_{600} of 0.05 in LB medium (400 mL×2) supplemented with 100 µg/mL Carbenicillin. The cultures were grown at 37 °C until an OD_{600} of 0.5, induced with 1 mM IPTG (final concentration) and grown for an additional 2 hours at 30 °C. The cells were harvested by centrifugation and resuspended in 20 ml of resuspension buffer (buffer I; 1 M KCl, 5 mM $MgCl_2$, 1 mM β-mercaptoethanol, 50 mM Tris:HCl pH 8.0) supplemented with 0.1 mM PMSF, 1 mg/ml lysozyme and 1 U/mL of DNase I and incubated on ice for 30 min. After adding 10 mL of lysis buffer (buffer J; 500 mM KCl, 500 mM NaCl, 1% glycerol, 1 mM β-mercaptoethanol, 50 mM Tris:HCl pH 8.0), cells were lysed by one passage through a high-pressure cell disrupter (Stansted Fluid Power, 150 MPa), cell debris was removed by centrifugation (25,000 rpm for 40 min, JA-25.50 Beckman Coulter rotor) and clarified lysate was taken for protein purification.

Clarified cell lysate was filtered through a 0.2 µm syringe filter and loaded onto the HisTrap 1 mL HP column pre-equilibrated in buffer K (500 mM KCl, 500 mM NaCl, 10 mM $MgCl_2$, 1 mM β-mercaptoethanol, 0.002% mellitic acid, 15 mM imidazole, 50 mM Tris:HCl pH 8.0). The column was washed with 5 CV of buffer K, and the protein was eluted with a linear gradient (20 CV, 0-100% buffer L) of buffer L (500 mM KCl, 500 mM NaCl, 10 mM $MgCl_2$, 1 mM β-mercaptoethanol, 0.002% mellitic acid, 500 mM imidazole, 50 mM Tris:HCl

826 pH 8.0). Fractions most enriched in His_6-TEV-MESH1 (≈50-60% buffer B) were pooled,
827 totalling approximately 3 mL. The sample was loaded on a HiLoad 16/600 Superdex 200 pg
828 column pre-equilibrated with buffer M (500 mM KCl, 500 mM NaCl, 10 mM $MgCl_2$, 1 mM β-
829 mercaptoethanol, 0.002% mellitic acid, 50 mM Tris:HCl pH 8.0). The fractions containing
830 His_6-TEV-MESH1 were pooled and subjected to buffer exchange by repeated filtration with an
831 Amicon Ultra (Millipore) centrifugal filter device (cut-off 15 kDa) pre-equilibrated in buffer N
832 (100 mM NaCl, 5 mM $MgCl_2$, 10% glycerol, 25 mM HEPES:KOH pH 7.5). The His-tag was
833 cleaved off by adding TEV protease in a 1:100 molar ratio and the reaction mixture was
834 incubated at 10 °C for overnight. After the His6 tag was cleaved off, the protein was passed
835 though 1 mL HisTrap HP pre-equilibrated with buffer N. Fractions containing MESH1 in the
836 flow-through were collected and concentrated on Amicon Ultra (Millipore) centrifugal filter
837 device with 15 kDa cut-off (final concentration is 4.75 µM). The purity of protein preparations
838 was assessed by SDS-PAGE and spectrophotometrically (OD_{260}/OD_{280} ratio below 0.5). Protein
839 preparations were aliquoted, frozen in liquid nitrogen and stored at –80 °C.
840
841 *C. marina* ATfaRel (VHp313, pET24d-His6-aTfaRel) was overexpressed in freshly
842 transformed *E. coli* BL21 DE3. Fresh transformants were inoculated to final OD_{600} of 0.05 in
843 the LB medium (800 mL) supplemented with 100 µg/mL kanamycin. The cultures were grown
844 at 37 °C until an OD_{600} of 0.5, induced with 0.4 mM IPTG (final concentration) and grown for
845 an additional one hour at 30 °C. The cells were harvested by centrifugation and resuspended in
846 30 ml of binding buffer (buffer O; 2 M NaCl, 5 mM $MgCl_2$, 70 µM $MnCl_2$, 50 mM arginine,
847 50 mM glutamic acid, 1 mM Mellitic acid, 20 mM imidazole, 10% glycerol, 4 mM β-
848 mercaptoethanol, 25 mM HEPES:KOH pH 7.6) supplemented with 0.1 mM PMSF and 1 U/mL
849 of DNase I, and cells were lysed by one passage through a high-pressure cell disrupter (Stansted
850 Fluid Power, 150 MPa), cell debris was removed by centrifugation (35,000 rpm for 45 min,
851 Type 45 Ti Beckman Coulter rotor) and clarified lysate was taken for protein purification.
852 Clarified cell lysate was filtered through a 0.2 µm syringe filter and loaded onto the
853 HisTrap 1 mL HP column pre-equilibrated in buffer O (2 M NaCl, 5 mM $MgCl_2$, 70 µM $MnCl_2$,
854 50 mM arginine, 50 mM glutamic acid, 1 mM Mellitic acid, 20 mM imidazole, 10% glycerol,
855 4 mM β-mercaptoethanol, 25 mM HEPES:KOH pH 7.6). The column was washed with 5 CV
856 of buffer O, and the protein was eluted with a linear gradient (10 CV, 0-100% buffer P) of
857 buffer P (2 M NaCl, 5 mM $MgCl_2$, 70 µM $MnCl_2$, 50 mM arginine, 50 mM glutamic acid, 1
858 mM Mellitic acid, 500 mM imidazole, 4 mM β-mercaptoethanol, 25 mM HEPES:KOH pH 7.6).
859 The fractions containing His_6-ATfaRel were pooled and subjected to buffer exchange by

repeated filtration with an Amicon Ultra (Millipore) centrifugal filter device (cut-off 3 kDa) pre-equilibrated in buffer Q (500 mM KCl, 5 mM $MgCl_2$, 50 mM arginine, 50 mM glutamic acid, 10% glycerol, 4 mM β-mercaptoethanol, 25 mM HEPES:KOH pH 8.0). The purity of protein preparations was assessed by SDS-PAGE. Protein preparations were aliquoted, frozen in liquid nitrogen and stored at –80 °C.

Preparation of *E. coli* fMet-tRNA$_i^{fMet}$ and tRNA^{Phe} modified by *Coprobacillus* sp. D7 FaRel2

fMet-tRNA$_i^{fMet}$ was prepared as described in before (Murina et al., 2018) using non-radioactive methionine.

To modify tRNA^{Phe}, the reaction mixture containing 5 µM tRNA^{Phe}, 500 µM ATP and 50 nM FaRel2-FLAG$_3$ in HEPES:Polymix buffer, pH 7.5 (Takada et al., 2020) (5 mM Mg^{2+} final concentration) supplemented with 1 mM DTT was incubated at 37 °C for 15 min. After that the reaction was supplemented with 0.1 volume of 3 M NaOAc (pH 4.6), the proteins were extracted with an equal volume of phenol/chloroform/isoamylalcohol (25:24:1), followed by a similar treatment with an equal volume of chloroform. As a negative control the same experiment was performed in the absence of FaRel2-FLAG$_3$. The extracted tRNA was mixed with 2.5 volume of 95 % ethanol, precipitated at –20 °C overnight and pelleted by centrifugation. The pellet was washed with 100 µL of ice-cold 70% ethanol, dried at room temperature for 5 minutes, and dissolved in 5 mM KOAc (pH 5.1). The concentration of the purified tRNA was calculated by measuring the absorbance at 260 nm, and phosphorylation was validated by aminoacylation reaction (see below).

Biochemical assays

Cell-free translation: experiments with PURExpress In Vitro Protein Synthesis Kit (NEB, E6800) were performed as per the manufacturer's instructions with the addition of 0.8 U/µL RNase Inhibitor Murine (NEB, M0314S). FaRel2-FLAG$_3$ was used at a final concentration of 50 nM, PhRel2-FLAG$_3$ at 100 nM and His$_6$-TEV-ATfaRel2 at 500 nM. As a control we used either HEPES:Polymix buffer, pH 7.5 (Takada et al., 2020) or eluate prepared from *E. coli* transformed with pBAD33 vector (mock). The total reaction volume was 6 µL per reaction for most of the experiments. To titrate the concentration of total tRNA in the reaction we used a combination of PURExpress Δ(aa, tRNA) Kit (NEB, E6840S) and total deacylated tRNA from *E. coli* MRE600 (Sigma-Aldrich, 10109541001). After incubation at 37 °C for the indicated time, the reaction mixture was mixed with 9-fold volume of 2x sample buffer (100 mM

Tris:HCl pH 6.8, 4% SDS, 0.02% bromophenol blue, 20% glycerol, 20 mM DTT and 4% β-mercaptoethanol), and 5 µL of the mixture was resolved on 18% SDS-PAGE gel. The SDS-PAGE gel was fixed by incubating for 5 min at room temperature in 50% ethanol solution supplemented with 2% phosphoric acid, then stained and detected as mentioned in protein expression and purification.

tRNA and oligonucleotide pyrophosphorylation by FaRel2: the reaction conditions are described above, see '*Preparation of E. coli fMet-tRNA*$_f^{fMet}$ *and tRNA*^{Phe} *modified by* Coprobacillus *sp. D7 FaRel2*'. PhRel2-FLAG$_3$ was used at a final concentration of 50 nM. Experiments with 5′-CACCN-3′ oligonucleotides used 50 µM oligonucleotides; tRNA (Chemical Block Ltd.) was used at a final concentration of 5 µM. The total reaction volume was either 8 or 20 µL per reaction. The reactions were started by the addition of 500 µM γ^{32}P-ATP and incubated at 37 °C for either 10 or 30 minutes. To calculate the ratio of phosphorylation, the reaction mixture was mixed in 10% trichloroacetic acid supplemented with 70 ng/µL *E. coli* total tRNA as co-precipitant, kept on ice for 30 minutes, and centrifuged at 21,000 g for 30 minutes at 4 °C. After washing the pellet with 200 µL 10% TCA, tRNA was dissolved in 1 M Tris:HCl (pH 8.0) with shaking at 1,500 rpm for 20 min at 4 °C. The radioactivity was quantified by scintillation counting in 5 mL of EcoLite Liquid Scintillation Cocktail (MP Biomedicals).

To visualise phosphorylated tRNA the reaction sample was mixed in 2 volumes of RNA dye (98% formamide, 10 mM EDTA, 0.3% bromophenol blue and 0.3% xylene cyanol), tRNA was denatured at 37 °C for 10 min and resolved on urea-PAGE in 1 x TBE (8 M urea, 8% PAGE). The gel was stained with SYBR Gold (Life technologies, S11494) and exposed to an imaging plate overnight. The imaging plate was imaged by a Typhoon FLA 9500 (GE Healthcare). To visualise phosphorylated oligonucleotides the sample was resolved on urea-PAGE in 1 x TBE (5.6 M urea, 24% PAGE).

Effects of pyrophosphorylation by FaRel2 on tRNA aminoacylation: to probe the effect of FaRel2 on aminoacylation, 5 µM *E. coli* tRNA^{Phe} (Chemical Block Ltd.) was pre-incubated at 37 °C with or without 50 nM FaRel2 as well as 500 µM ATP for 10 minutes in HEPES:Polymix buffer, pH 7.5 (Takada et al., 2020) (5 mM Mg^{2+} final concentration) supplemented with 1 mM DTT and 160 µM ^{3}H-phenylalanine. The total reaction volume was 20 µL. The tRNA was then aminoacylated by adding the same volume of aminoacylation mixture (4 mM ATP and 2 µM PheRS in HEPES:Polymix buffer (5 mM Mg^{2+} final concentration), 1 mM DTT) followed by

additional incubation at 37 °C for 10 minutes. The reaction was quenched by adding trichloroacetic acid (TCA) to a final concentration of 10% as well as adding 70 ng/µL *E. coli* total tRNA as co-precipitant. After 30-minute incubation on ice, the tRNA was pelleted by centrifugation (21,000 g for 30 minutes at 4 °C). The supernatant was discarded, the pellet washed with 10% TCA and the tRNA was dissolved in 1 M Tris:HCl (pH 8.0) with shaking at 1,500 rpm for 20 min at 4 °C. Finally, ^{3}H-radioactivity was quantified by scintillation counting in 5 mL of EcoLite Liquid Scintillation Cocktail (MP Biomedicals).

In the case of experiments using SAH enzymes, 5 µM $tRNA^{Phe}$ with or without modification by FaRel2-$FLAG_3$ was pre-incubated for 10 minutes with or without 1 µM MESH1, His_6-ATfaRel or His_6-TEV-ATfaRel2 at 37 °C in HEPES:Polymix buffer pH 7.5 (5 mM Mg^{2+} final concentration) (Takada et al., 2020) additionally supplemented with 1 mM $MnCl_2$, 160 µM ^{3}H-phenylalanine and 1 mM DTT. After 10 minute PheRS was added to final concentration of 1 µM and after additional 10 minutes at 37 °C the reaction was quenched by TCA and incorporation of the ^{3}H-radioactivity was quantified by scintillation counting (see above).

^{3}H-ppGpp synthesis by E. coli *RelA*: *E. coli* RelA synthase activity assay was performed in HEPES:Polymix buffer (5 mM Mg^{2+} final concentration) as described earlier (Takada et al., 2020) with minor modifications. Specifically, the assay was performed in the presence of 300 µM ^{3}H-GDP, 1 mM ATP, 100 µM pppGpp, 50 nM native RelA and 100 nM 70S IC(MVF), in the presence or absence of 100 nM *E. coli* deacylated $tRNA^{Val}$ (Chemical Block Ltd.); 5 µL total reaction volume per timepoint. *E. coli* deacylated $tRNA^{Val}$ and ATP were initially incubated with either HEPES:Polymix buffer, empty vector lysate, or lysate containing FaRel2, at 37 °C for 30 minutes. GDP, pppGpp, and 70S IC were then added and the reactions were started by the addition of RelA. Subsequently, aliquots were withdrawn from the reaction mix, resolved on PEI-TLC, radioactivity quantified by scintillation counting and the turnovers were determined as previously described (Turnbull et al., 2019).

Structural modelling and docking

The structure of FaRel2 was modelled using Rosetta (Song et al., 2013) based on the coordinates of *S. aureus* RelP (Manav et al., 2018) and *B. subtilis* RelQ (Steinchen et al., 2015). The models with the best scores were used for molecular docking as implemented in the web server version of HADDOCK (High ambiguity driven biomolecular docking) (van Zundert et al., 2016) together with the coordinates of yeast $tRNA^{Phe}$ (Nissen et al., 1995).

For the docking procedure we defined residues in the active site; Y128 and the catalytic glutamine were selected as active residues (i.e. directly involved in the interaction). We then allowed HADDOCK to automatically select passive residues around the active residues. The program was run with default settings. The best cluster resulting from the docking experiment was selected to further probe the catalytic mechanism of FaRel2.

Figure preparation

Figures were prepared using UCSF ChimeraX (Goddard et al., 2018), Igor Pro (WaveMetrics, Inc.), Adobe Illustrator (Adobe Inc.) and Adobe Photoshop (Adobe Inc.).

QUANTIFICATION AND STATISTICAL ANALYSIS

Statistical analysis of tRNA aminoacylation, tRNA pyrophosphorylation and ^{3}H-ppGpp synthesis data was performed using Igor Pro (WaveMetrics, Inc.). The data was plotted as individual data points as well as mean values ± standard deviations.

DATA AND SOFTWARE AVAILABILITY

The study does not make use of unpublished data or software.

RESOURCES TABLE

REAGENT or RESOURCE	SOURCE	IDENTIFIER
Antibodies		
Anti-Flag M2 primary antibodies (1:5,000)	Sigma-Aldrich	Cat#F1804 RRID: AB_262044
Anti-mouse-HRP secondary antibodies (1:10,000)	Rockland	Cat#610-103-040 RRID: AB_2614833
Bacterial strains		
Escherichia coli BW25113	(Grenier et al., 2014)	N/A
E. coli DH5α	Laboratory stock	N/A
For other *E. coli* strains see Table S1	N/A	N/A
Chemicals, Peptides, and Recombinant Proteins		
Anti-FLAG M2 Affinity Gel	Sigma-Aldrich	Cat#A2220-25ML RRID:AB_10063035
Poly FLAG Peptide lyophilized powder	Bimake	Cat#B23112
Phusion High-Fidelity PCR Master Mix with HF Buffer	Thermo Scientific	Cat#F531L
Q5® High-Fidelity DNA Polymerase	New England Biolabs	Cat#M0491L
DpnI	New England Biolabs	Cat#R0176S
T4 DNA Ligase	New England Biolabs	Cat#M0202S

NEBuilder® HiFi DNA Assembly Master Mix	New England Biolabs	Cat#E2621L
L-[^{35}S]-Methionine	PerkinElmer	Cat#NEG009C005MC
[5,6-^{3}H]-Uridine	PerkinElmer	Cat#NET367250UC
[Methyl-^{3}H]-Thymidine	PerkinElmer	Cat#NET027W001MC
ATP, [γ-^{32}P]- 3000Ci/mmol 10mCi/ml EasyTide Lead	PerkinElmer	Cat#NEG502A500UC
L-[2,3,4,5,6-3H]-Phenylalanine	PerkinElmer	Cat#NET1122001MC
EcoLite™ Liquid Scintillation Cocktail	MP Biomedicals	Cat#01882475-CF
TEV protease	Protein Expertise Platform at Umeå University	N/A
PURExpress In Vitro Protein Synthesis Kit	New England Biolabs	Cat#E6800
PURExpress Δ(aa, tRNA) Kit	New England Biolabs	Cat#E6840S
RNase Inhibitor Murine	New England Biolabs	Cat#M0314S
pppGpp	(Takada et al., 2020)	N/A
pApp	This work	N/A
ppApp	(Jimmy et al., 2020)	N/A
pppApp	This work	N/A
^{3}H-ppGpp	(Takada et al., 2020)	N/A
70S initiation complex (IC) (MVF)	(Takada et al., 2020)	N/A
WesternBright Quantum	Advansta	Cat#K-12042-D10
cOmplete EDTA-free Protease Inhibitor Cocktail	Roche	Cat#4693132001
E. coli tRNA^{Phe}	Chemical Block	N/A
E. coli tRNA^{Val}	Chemical Block	N/A
E. coli tRNA$_i^{Met}$	Chemical Block	N/A
Oligonucleotides		
For primers used for cloning of *E. coli* plasmids see Table S1	N/A	N/A
5′ rCrArCrCrA 3′	Integrated DNA Technologies	N/A
5′ rCrArCrCrU 3′	Integrated DNA Technologies	N/A
5′ rCrArCrCrG 3′	Integrated DNA Technologies	N/A
5′ rCrArCrCrC 3′	Integrated DNA Technologies	N/A
5′ dCdAdCdCdA 3′	Integrated DNA Technologies	N/A
Recombinant DNA		
For *E. coli* vectors see Table S1	This work	N/A
Software and Algorithms		
Rosetta	(Song et al., 2013)	RRID:SCR_015701
HADDOCK	(van Zundert et al., 2016)	RRID:SCR_019091
MAFFT	(Katoh and Standley, 2013)	RRID:SCR_011811
Jalview	(Waterhouse et al., 2009)	RRID:SCR_006459

UCSF ChimeraX	(Goddard et al., 2018)	RRID:SCR_015872
Other		
FastPrep-24 classic	MP Biomedicals	https://www.mpbio.com
Biocomp Gradient Station	BioComp Instruments	http://www.biocompinstruments.com
Trans-Blot Turbo 0.2 µm Midi Nitrocellulose Transfer Pack	Bio-Rad	Cat#1704159
ImageQuant LAS 4000	GE Healthcare	https://www.cytivalifesciences.com
Mix2Seq sequencing service	Eurofins Genomics	https://www.eurofinsgenomics.eu
Micro Bio-Spin Columns	Bio-Rad	Cat#7326204
Typhoon FLA 9500	GE Healthcare	https://www.cytivalifesciences.com
0.1 mm Zirconium beads	BioSpec	Cat#11079101z
Multi-Purpose Tube Rotators	Fisherbrand™	https://www.fishersci.com
Micro Bio-Spin Columns	Bio-Rad	Cat#7326204
HisTrap 1 mL HP column	GE Healthcare	Cat#17-5247-01
HisTrap 5 mL HP column	GE Healthcare	Cat#17-5248-01
HiPrep 10/26 desalting column	GE Healthcare	Cat#17-5087-01
HiLoad 16/600 Superdex 200 pg column	GE Healthcare	Cat#28-9893-35
POLYGRAM CEL 300 PEI	Machery Nagel	Cat#801053, Lot#01.17
ÄKTA avant 25	GE Healthcare	https://www.cytivalifesciences.com

DATA AND SOFTWARE AVAILABILITY

Sequences shown in the multiple sequence alignment of **Figure S5A** can be downloaded from the Uniprot database (https://www.uniprot.org/) in case of Rel and RelA, and the NCBI protein database for all other sequences, using the accession numbers shown in the figure.

REFERENCES

Ahmad, S., Wang, B., Walker, M.D., Tran, H.R., Stogios, P.J., Savchenko, A., Grant, R.A., McArthur, A.G., Laub, M.T., and Whitney, J.C. (2019). An interbacterial toxin inhibits target cell growth by synthesizing (p)ppApp. Nature *575*, 674-678.

Arenz, S., Abdelshahid, M., Sohmen, D., Payoe, R., Starosta, A.L., Berninghausen, O., Hauryliuk, V., Beckmann, R., and Wilson, D.N. (2016). The stringent factor RelA adopts an open conformation on the ribosome to stimulate ppGpp synthesis. Nucleic Acids Res *44*, 6471-6481.

Atkinson, G.C., Tenson, T., and Hauryliuk, V. (2011). The RelA/SpoT homolog (RSH) superfamily: distribution and functional evolution of ppGpp synthetases and hydrolases across the tree of life. PLoS One *6*, e23479.

Blower, T.R., Fineran, P.C., Johnson, M.J., Toth, I.K., Humphreys, D.P., and Salmond, G.P. (2009). Mutagenesis and functional characterization of the RNA and protein components of the toxIN abortive infection and toxin-antitoxin locus of Erwinia. J Bacteriol *191*, 6029-6039.

Brosius, J., and Holy, A. (1984). Regulation of ribosomal RNA promoters with a synthetic lac operator. Proc Natl Acad Sci U S A *81*, 6929-6933.

Brown, A., Fernandez, I.S., Gordiyenko, Y., and Ramakrishnan, V. (2016). Ribosome-dependent activation of stringent control. Nature *534*, 277-280.

Burckhardt, R.M., and Escalante-Semerena, J.C. (2020). Small-Molecule Acetylation by GCN5-Related N-Acetyltransferases in Bacteria. Microbiol Mol Biol Rev *84*.

Cai, Y., Usher, B., Gutierrez, C., Tolcan, A., Mansour, M., Fineran, P.C., Condon, C., Neyrolles, O., Genevaux, P., and Blower, T.R. (2020). A nucleotidyltransferase toxin inhibits growth of Mycobacterium tuberculosis through inactivation of tRNA acceptor stems. Sci Adv *6*, eabb6651.

Candiano, G., Bruschi, M., Musante, L., Santucci, L., Ghiggeri, G.M., Carnemolla, B., Orecchia, P., Zardi, L., and Righetti, P.G. (2004). Blue silver: a very sensitive colloidal Coomassie G-250 staining for proteome analysis. Electrophoresis *25*, 1327-1333.

Cashel, M., and Gallant, J. (1969). Two compounds implicated in the function of the RC gene of Escherichia coli. Nature *221*, 838-841.

Castro-Roa, D., Garcia-Pino, A., De Gieter, S., van Nuland, N.A., Loris, R., and Zenkin, N. (2013). The Fic protein Doc uses an inverted substrate to phosphorylate and inactivate EF-Tu. Nat Chem Biol *9*, 811-817.

Cheverton, A.M., Gollan, B., Przydacz, M., Wong, C.T., Mylona, A., Hare, S.A., and Helaine, S. (2016). A Salmonella Toxin Promotes Persister Formation through Acetylation of tRNA. Mol Cell *63*, 86-96.

Cruz, J.W., Sharp, J.D., Hoffer, E.D., Maehigashi, T., Vvedenskaya, I.O., Konkimalla, A., Husson, R.N., Nickels, B.E., Dunham, C.M., and Woychik, N.A. (2015). Growth-regulating Mycobacterium tuberculosis VapC-mt4 toxin is an isoacceptor-specific tRNase. Nat Commun *6*, 7480.

Dedrick, R.M., Jacobs-Sera, D., Bustamante, C.A., Garlena, R.A., Mavrich, T.N., Pope, W.H., Reyes, J.C., Russell, D.A., Adair, T., Alvey, R.*, et al.* (2017). Prophage-mediated defence against viral attack and viral counter-defence. Nat Microbiol *2*, 16251.

Ding, C.C., Rose, J., Sun, T., Wu, J., Chen, P.H., Lin, C.C., Yang, W.H., Chen, K.Y., Lee, H., Xu, E.*, et al.* (2020). MESH1 is a cytosolic NADPH phosphatase that regulates ferroptosis. Nat Metab *2*, 270-277.

Fiedoruk, K., Daniluk, T., Swiecicka, I., Sciepuk, M., and Leszczynska, K. (2015). Type II toxin-antitoxin systems are unevenly distributed among Escherichia coli phylogroups. Microbiology (Reading) *161*, 158-167.

Fraikin, N., Goormaghtigh, F., and Van Melderen, L. (2020). Type II Toxin-Antitoxin Systems: Evolution and Revolutions. J Bacteriol *202*.

Gaca, A.O., Colomer-Winter, C., and Lemos, J.A. (2015). Many means to a common end: the intricacies of (p)ppGpp metabolism and its control of bacterial homeostasis. J Bacteriol *197*, 1146-1156.

Garcia-Pino, A., Zenkin, N., and Loris, R. (2014). The many faces of Fic: structural and functional aspects of Fic enzymes. Trends Biochem Sci *39*, 121-129.

Geiger, T., Kastle, B., Gratani, F.L., Goerke, C., and Wolz, C. (2014). Two small (p)ppGpp synthases in Staphylococcus aureus mediate tolerance against cell envelope stress conditions. J Bacteriol *196*, 894-902.

Goddard, T.D., Huang, C.C., Meng, E.C., Pettersen, E.F., Couch, G.S., Morris, J.H., and Ferrin, T.E. (2018). UCSF ChimeraX: Meeting modern challenges in visualization and analysis. Protein Sci *27*, 14-25.

Goeders, N., Dreze, P.L., and Van Melderen, L. (2013). Relaxed cleavage specificity within the RelE toxin family. J Bacteriol *195*, 2541-2549.

Grenier, F., Matteau, D., Baby, V., and Rodrigue, S. (2014). Complete Genome Sequence of Escherichia coli BW25113. Genome Announc *2*.

Guzman, L.M., Belin, D., Carson, M.J., and Beckwith, J. (1995). Tight regulation, modulation, and high-level expression by vectors containing the arabinose PBAD promoter. J Bacteriol *177*, 4121-4130.

Harms, A., Brodersen, D.E., Mitarai, N., and Gerdes, K. (2018). Toxins, Targets, and Triggers: An Overview of Toxin-Antitoxin Biology. Mol Cell *70*, 768-784.

Harms, A., Stanger, F.V., Scheu, P.D., de Jong, I.G., Goepfert, A., Glatter, T., Gerdes, K., Schirmer, T., and Dehio, C. (2015). Adenylylation of Gyrase and Topo IV by FicT Toxins Disrupts Bacterial DNA Topology. Cell Rep *12*, 1497-1507.

Haseltine, W.A., and Block, R. (1973). Synthesis of guanosine tetra- and pentaphosphate requires the presence of a codon-specific, uncharged transfer ribonucleic acid in the acceptor site of ribosomes. Proc Natl Acad Sci U S A *70*, 1564-1568.

Hauryliuk, V., Atkinson, G.C., Murakami, K.S., Tenson, T., and Gerdes, K. (2015). Recent functional insights into the role of (p)ppGpp in bacterial physiology. Nat Rev Microbiol *13*, 298-309.

Irving, S.E., Choudhury, N.R., and Corrigan, R.M. (2020). The stringent response and physiological roles of (pp)pGpp in bacteria. Nat Rev Microbiol.

Jaffe, A., Ogura, T., and Hiraga, S. (1985). Effects of the ccd function of the F plasmid on bacterial growth. J Bacteriol *163*, 841-849.

Jaskolska, M., and Gerdes, K. (2015). CRP-dependent positive autoregulation and proteolytic degradation regulate competence activator Sxy of Escherichia coli. Mol Microbiol *95*, 833-845.

Jimmy, S., Saha, C.K., Kurata, T., Stavropoulos, C., Oliveira, S.R.A., Koh, A., Cepauskas, A., Takada, H., Rejman, D., Tenson, T.*, et al.* (2020). A widespread toxin-antitoxin system exploiting growth control via alarmone signaling. Proc Natl Acad Sci U S A *117*, 10500-10510.

Jurenaite, M., Markuckas, A., and Suziedeliene, E. (2013). Identification and characterization of type II toxin-antitoxin systems in the opportunistic pathogen Acinetobacter baumannii. J Bacteriol *195*, 3165-3172.

Jurenas, D., Chatterjee, S., Konijnenberg, A., Sobott, F., Droogmans, L., Garcia-Pino, A., and Van Melderen, L. (2017). AtaT blocks translation initiation by N-acetylation of the initiator tRNA(fMet). Nat Chem Biol *13*, 640-646.

Katoh, K., and Standley, D.M. (2013). MAFFT multiple sequence alignment software version 7: improvements in performance and usability. Mol Biol Evol *30*, 772-780.

Koonin, E.V., and Makarova, K.S. (2019). Origins and evolution of CRISPR-Cas systems. Philos Trans R Soc Lond B Biol Sci *374*, 20180087.

Kudrin, P., Dzhygyr, I., Ishiguro, K., Beljantseva, J., Maksimova, E., Oliveira, S.R.A., Varik, V., Payoe, R., Konevega, A.L., Tenson, T., *et al.* (2018). The ribosomal A-site finger is crucial for binding and activation of the stringent factor RelA. Nucleic Acids Res *46*, 1973-1983.

Kudrin, P., Varik, V., Oliveira, S.R., Beljantseva, J., Del Peso Santos, T., Dzhygyr, I., Rejman, D., Cava, F., Tenson, T., and Hauryliuk, V. (2017). Subinhibitory Concentrations of Bacteriostatic Antibiotics Induce relA-Dependent and relA-Independent Tolerance to beta-Lactams. Antimicrob Agents Chemother *61*.

Lima-Mendez, G., Oliveira Alvarenga, D., Ross, K., Hallet, B., Van Melderen, L., Varani, A.M., and Chandler, M. (2020). Toxin-Antitoxin Gene Pairs Found in Tn3 Family Transposons Appear To Be an Integral Part of the Transposition Module. mBio *11*.

Liu, K., Bittner, A.N., and Wang, J.D. (2015). Diversity in (p)ppGpp metabolism and effectors. Curr Opin Microbiol *24*, 72-79.

Loveland, A.B., Bah, E., Madireddy, R., Zhang, Y., Brilot, A.F., Grigorieff, N., and Korostelev, A.A. (2016). Ribosome*RelA structures reveal the mechanism of stringent response activation. Elife *5*.

Manav, M.C., Beljantseva, J., Bojer, M.S., Tenson, T., Ingmer, H., Hauryliuk, V., and Brodersen, D.E. (2018). Structural basis for (p)ppGpp synthesis by the Staphylococcus aureus small alarmone synthetase RelP. J Biol Chem *293*, 3254-3264.

Murina, V., Kasari, M., Hauryliuk, V., and Atkinson, G.C. (2018). Antibiotic resistance ABCF proteins reset the peptidyl transferase centre of the ribosome to counter translational arrest. Nucleic Acids Res *46*, 3753-3763.

Nanamiya, H., Kasai, K., Nozawa, A., Yun, C.S., Narisawa, T., Murakami, K., Natori, Y., Kawamura, F., and Tozawa, Y. (2008). Identification and functional analysis of novel (p)ppGpp synthetase genes in Bacillus subtilis. Mol Microbiol *67*, 291-304.

Neidhardt, F.C., Bloch, P.L., and Smith, D.F. (1974). Culture medium for enterobacteria. J Bacteriol *119*, 736-747.

Nissen, P., Kjeldgaard, M., Thirup, S., Polekhina, G., Reshetnikova, L., Clark, B.F., and Nyborg, J. (1995). Crystal structure of the ternary complex of Phe-tRNAPhe, EF-Tu, and a GTP analog. Science *270*, 1464-1472.

Page, R., and Peti, W. (2016). Toxin-antitoxin systems in bacterial growth arrest and persistence. Nat Chem Biol *12*, 208-214.

Patil, P.R., Vithani, N., Singh, V., Kumar, A., and Prakash, B. (2020). A revised mechanism for (p)ppGpp synthesis by Rel proteins: The critical role of the 2'-OH of GTP. J Biol Chem *295*, 12851-12867.

Schattenkerk, C., Wreesmann, C.T., van der Marel, G.A., and van Boom, J.H. (1985). Synthesis of riboguanosine pentaphosphate ppprGpp (Magic Spot II) via a phosphotriester approach. Nucleic Acids Res *13*, 3635-3649.

Schneider, C.A., Rasband, W.S., and Eliceiri, K.W. (2012). NIH Image to ImageJ: 25 years of image analysis. Nat Methods *9*, 671-675.

Schureck, M.A., Dunkle, J.A., Maehigashi, T., Miles, S.J., and Dunham, C.M. (2015). Defining the mRNA recognition signature of a bacterial toxin protein. Proc Natl Acad Sci U S A *112*, 13862-13867.

Senissar, M., Manav, M.C., and Brodersen, D.E. (2017). Structural conservation of the PIN domain active site across all domains of life. Protein Sci *26*, 1474-1492.

Shimizu, Y., Inoue, A., Tomari, Y., Suzuki, T., Yokogawa, T., Nishikawa, K., and Ueda, T. (2001). Cell-free translation reconstituted with purified components. Nat Biotechnol *19*, 751-755.

Song, S., and Wood, T.K. (2020). A Primary Physiological Role of Toxin/Antitoxin Systems Is Phage Inhibition. Front Microbiol *11*, 1895.

Song, Y., DiMaio, F., Wang, R.Y., Kim, D., Miles, C., Brunette, T., Thompson, J., and Baker, D. (2013). High-resolution comparative modeling with RosettaCM. Structure *21*, 1735-1742.

Sprinzl, M., and Richter, D. (1976). Free 3'-OH group of the terminal adenosine of the tRNA molecule is essential for the synthesis in vitro of guanosine tetraphosphate and pentaphosphate in a ribosomal system from Escherichia coli. Eur J Biochem *71*, 171-176.

Steinchen, W., Schuhmacher, J.S., Altegoer, F., Fage, C.D., Srinivasan, V., Linne, U., Marahiel, M.A., and Bange, G. (2015). Catalytic mechanism and allosteric regulation of an oligomeric (p)ppGpp synthetase by an alarmone. Proc Natl Acad Sci U S A *112*, 13348-13353.

Steinchen, W., Vogt, M.S., Altegoer, F., Giammarinaro, P.I., Horvatek, P., Wolz, C., and Bange, G. (2018). Structural and mechanistic divergence of the small (p)ppGpp synthetases RelP and RelQ. Sci Rep *8*, 2195.

Sun, D., Lee, G., Lee, J.H., Kim, H.Y., Rhee, H.W., Park, S.Y., Kim, K.J., Kim, Y., Kim, B.Y., Hong, J.I., *et al.* (2010). A metazoan ortholog of SpoT hydrolyzes ppGpp and functions in starvation responses. Nat Struct Mol Biol *17*, 1188-1194.

Takada, H., Roghanian, M., Murina, V., Dzhygyr, I., Murayama, R., Akanuma, G., Atkinson, G.C., Garcia-Pino, A., and Hauryliuk, V. (2020). The C-terminal RRM/ACT domain is crucial for fine-tuning the activation of 'long' RelA-SpoT Homolog enzymes by ribosomal complexes. Frontiers in microbiology *11*, 277.

Turnbull, K.J., Dzhygyr, I., Lindemose, S., Hauryliuk, V., and Roghanian, M. (2019). Intramolecular Interactions Dominate the Autoregulation of Escherichia coli Stringent Factor RelA. Front Microbiol *10*, 1966.

van Zundert, G.C.P., Rodrigues, J., Trellet, M., Schmitz, C., Kastritis, P.L., Karaca, E., Melquiond, A.S.J., van Dijk, M., de Vries, S.J., and Bonvin, A. (2016). The HADDOCK2.2 Web Server: User-Friendly Integrative Modeling of Biomolecular Complexes. J Mol Biol *428*, 720-725.

Varik, V., Oliveira, S.R.A., Hauryliuk, V., and Tenson, T. (2017). HPLC-based quantification of bacterial housekeeping nucleotides and alarmone messengers ppGpp and pppGpp. Sci Rep *7*, 11022.

Waterhouse, A.M., Procter, J.B., Martin, D.M., Clamp, M., and Barton, G.J. (2009). Jalview Version 2--a multiple sequence alignment editor and analysis workbench. Bioinformatics *25*, 1189-1191.

Winther, K.S., and Gerdes, K. (2011). Enteric virulence associated protein VapC inhibits translation by cleavage of initiator tRNA. Proc Natl Acad Sci U S A *108*, 7403-7407.

Xiao, H., Kalman, M., Ikehara, K., Zemel, S., Glaser, G., and Cashel, M. (1991). Residual guanosine 3',5'-bispyrophosphate synthetic activity of relA null mutants can be eliminated by spoT null mutations. J Biol Chem *266*, 5980-5990.

Yamaguchi, Y., and Inouye, M. (2009). mRNA interferases, sequence-specific endoribonucleases from the toxin-antitoxin systems. Prog Mol Biol Transl Sci *85*, 467-500.

Zhu, M., Pan, Y., and Dai, X. (2019). (p)ppGpp: the magic governor of bacterial growth economy. Curr Genet *65*, 1121-1125.